INFORMATION TO USERS

The most advanced technology has been used to photograph and reproduce this manuscript from the microfilm master. UMI films the text directly from the original or copy submitted. Thus, some thesis and dissertation copies are in typewriter face, while others may be from any type of computer printer.

The quality of this reproduction is dependent upon the quality of the copy submitted. Broken or indistinct print, colored or poor quality illustrations and photographs, print bleedthrough, substandard margins, and improper alignment can adversely affect reproduction.

In the unlikely event that the author did not send UMI a complete manuscript and there are missing pages, these will be noted. Also, if unauthorized copyright material had to be removed, a note will indicate the deletion.

Oversize materials (e.g., maps, drawings, charts) are reproduced by sectioning the original, beginning at the upper left-hand corner and continuing from left to right in equal sections with small overlaps. Each original is also photographed in one exposure and is included in reduced form at the back of the book. These are also available as one exposure on a standard 35mm slide or as a 17" x 23" black and white photographic print for an additional charge.

Photographs included in the original manuscript have been reproduced xerographically in this copy. Higher quality 6" x 9" black and white photographic prints are available for any photographs or illustrations appearing in this copy for an additional charge. Contact UMI directly to order.

U·M·I

University Microfilms International
A Bell & Howell Information Company
300 North Zeeb Road, Ann Arbor, MI 48106-1346 USA
313/761-4700 800/521-0600

Order Number 8914755

Raman optical activity

Gunnia, Umamaheswari B., Ph.D.

City University of New York, 1988

U·M·I
300 N. Zeeb Rd.
Ann Arbor, MI 48106

RAMAN OPTICAL ACTIVITY

BY

UMAMAHESWARI. B. GUNNIA

A dissertation submitted to the Graduate Faculty in Chemistry in partial fulfillment of the requirements for the degree of Doctor of Philosophy, The City University of New York.

1988

This manuscript has been read and accepted for the Graduate Faculty in Chemistry in satisfaction of the dissertation requirement for the degree of Doctor of Philosophy.

5/6/88
Date

Chair of Examining Committee

5/6/88
Date

Executive Officer

Professor Daniel Akins

Professor Louis Massa

Professor Richard Mendelsohn

Supervisory Committee

The City University of New York

To my husband and children, whose support and cooperation meant a lot to the completion of this work.

Abstract

RAMAN OPTICAL ACTIVITY

by

Umamaheswari. B. Gunnia

Adviser: Professor Max Diem

In this thesis, different aspects of the ROA technique are explored. An attempt is made at the theoretical understanding of the phenomenon via both the classical and quantum mechanical approaches. Instrumental improvements of the system in recent years with emphasis on new, better and faster alignment procedures are a major part of this work. Understanding and elimination of the various artefacts in ROA are achieved with the hope of establishing the technique as a usable analytical tool. New data presented will speak of the success and also the limitations of this challenging experiment.

ACKNOWLEDGMENT

My first and foremost thanks go to Prof. Max Diem, my thesis advisor on this work. His ever-available suggestions and discussions have been quite valuable for me throughout the course of this study. I am extremely grateful for his overwhelming encouragement and support. I owe him special thanks for his patience and the time he spent in discussions during the writing of this thesis. I also thank Dr. Mark Davies for teaching me the "tricks of the trade" and my colleague, Ou Lee, for all his help.

TABLE OF CONTENTS

LIST OF TABLES

LIST OF FIGURES

INTRODUCTION

A. Objective and approach of the research

Optical activity, which is the differential interaction of left and right circularly polarized light with certain matter, is a unique molecular property exhibited by chiral media. Chiroptical techniques, which measure the above-mentioned differential interaction, have gained popularity as tools for structural elucidation -configurational as well as conformational- although the correlation between optical activity data and structural information, is, by no means, trivial. The fact that many important biological molecules like proteins, enzymes and peptides are optically active has brought about the collaboration of biochemists and chemists in exploiting these techniques to their fullest extent. Vibrational optical activity (VOA), which is the subject of this dissertation, is at present one of the novel chiroptical methods available for structural elucidation of chiral molecules. It encompasses both vibrational circular dichroism (VCD) as well as Raman optical activity (ROA).

The main objective of the research work undertaken here is to explore the potentials of ROA for stereochemical applications. The weak signals and overwhelming artefacts accompanying the experiment have repelled chemists from utilizing this technique. The aim of this study was the further development of ROA instrumentation, including new

systematic and computer-aided alignment programs to give better instrument alignments within shorter time-periods, and make the collection of reliable ROA data almost inevitable. The sources of the various problems have been thoroughly investigated, and successful solutions are cited. In addition, several modifications have been made in the ROA instrument, and interesting positive features have been added. Strength of the new set-up and success of the changes introduced are demonstrated with the aid of newly collected ROA data.

B. Significance

Conventional chiroptical methods, such as electronic circular dichroism (CD) and optical rotatory dispersion (ORD), have served as tools for structural analysis of chiral molecules for more than 25 years. They are powerful stereochemical probes and are quite sensitive to small changes in conformation. Unlike the situation in X-ray crystallography, solid samples are not necessary in these methods and liquids and solutions can be routinely studied. Structural data on solutions are needed since solvation can influence the conformation of a compound between solution and solid phases. Moreover, powerful spectroscopic methods, such as Nuclear Magnetic Resonance (NMR), cannot probe the chirality of optically active compounds directly. However, as with any other method, CD and ORD have their own limitations. In CD, a chromophore exhibiting an accessible elect-

ronic transition is needed; CD probes the chiral perturbation of such chromophores. However, not all molecules have low-lying electronic transitions in the ultraviolet UV/visible region. Moreover, for large molecules with chiral center away from the chromophore, the method fails to give any observable CD. For molecules absorbing in the far UV, tedious vacuum techniques have to be employed. ORD may be observed even far from transitions, but as a superposition of all the transitions. Thus, the effect lacks selectivity. Another main drawback of electronic CD and ORD is the broad and diffuse nature of the bands which make any theoretical modeling of the spectra difficult.

The above mentioned problems encountered in ORD and CD led chemists to think of alternatives. Chemists foresaw that VOA could give much more and novel information than electronic optical activity methods, in a similar way as vibrational spectroscopy is more informative than electronic spectroscopy. It could have all the advantages of electronic optical activity techniques and more.

Extension of CD into the infrared (IR) region was logically the first VOA technique to be developed. In VCD, the differences in the absorption of left and right circularly polarized IR radiation by chiral molecules, defined as

$$\Delta A = A_L - A_R \qquad (I.1)$$

is measured. "A" refers to the absorbance, capital subscripts R and L are used here and henceforth to denote

right and left circular polarized light, respectively.

ROA was anticipated as early as 1935. ROA is a light scattering phenomenon. Chiral molecules scatter left and right circularly polarized light to different extents; the normalised scattering differential given by

$$\Delta = (I_L - I_R) / (I_L + I_R) \qquad (I.2)$$

is the measured parameter in ROA. Here, "I" represents the scattered Raman intensity.

In VOA, nuclear configuration is probed; the chromophores involved exhibit vibrational and not electronic transitions. Because there are (3N-6) vibrational degrees of freedom available for nonlinear molecules (where N is the number of atoms in a molecule), any and every portion of the molecule can be studied. The transitions are fairly well resolved and are easy to assign, at least for most medium size molecules. Because the vibrations extend over the entire molecule, the method is very sensitive to subtle conformational changes in molecules.

VCD and ROA measure intensities that are quite small ($\Delta A/A$ or Δ are of the order of 10^{-4} or less). Both ROA and VCD have developed in a parallel fashion theoretically and experimentally and, at present, provide complementary structural information. VCD, at present is capable of penetrating down to about 600 cm^{-1} and is excellent in probing the region above 1000 cm^{-1} where many fundamental stretching modes occur. ROA, on the other hand covers the entire vibrational spectrum from 50-4000 cm^{-1}. ROA is at

its very best in the low frequency region. This is the region where interesting skeletal deformations and torsional modes occur which carry direct structural information. This region is at present not accessible via VCD. Other advantages of ROA over VCD are the following: First, optical activity depends on the frequency of the exciting light, and vibrational frequencies are an order of magnitude smaller than frequencies of visible light. In ROA the sample is excited with visible light; therefore, ROA intensities are comparatively larger. Secondly, biological application is one of the primary goals of VOA. Water is the natural medium for biological species and aqueous solutions are better studied via ROA than VCD. Water is a poor scattering medium but it is one of the strongest absorbers of IR radiation. Thus ROA may hold great promises as a structural probe for optically active molecules including interesting biological species. It is expected that, in the low frequency region which is unavailable to VCD, the structural information provided by ROA cannot be surpassed.

II. BACKGROUND

A. History of natural optical activity

Interaction of light and matter has been the subject of interest for physicists and chemists for a long time. Scientists have been studying the different properties of radiation - its intensity, frequency, phase etc.,- and how these properties change as a result of its interaction with matter. They have attempted to relate these changes to the structure of matter and design novel spectrochemical methods for structural elucidation.

Historically, natural optical activity is a phenomenon which was almost exclusively investigated by crystallographers and physicists, in the early nineteenth century. In 1809 polarization of light by reflection was discovered by Malus in Paris (1). Subsequently, Arago performed an experiment with crystalline quartz and a rotatable calcite plate (1811). He passed white light along the optic axis of the crystal and saw that a range of colors emerged. Biot (2) repeated Arago's experiment. He explained the observation of different colors through the crystal as due to a unique property possessed by the quartz crystal. He found that a rotation of plane of polarization of light had occurred. He also observed that the rotation was nearly proportional to the inverse square of the wavelength and was a function of the thickness of the sample. The credit goes to Augustin Fresnel (1788-1827) for giving a physical

explanation for the optical activity phenomenon. He explained optical rotation on the hypothesis of a transverse light wave (the electric vector being perpendicular to the direction of propagation) and demonstrated mathematically that plane polarized rays can be decomposed into two circularly polarized rays rotating in the opposite directions. If the two rays travel inside the medium with different velocities, rotation of the plane of polarization results. He called the effect "circular double refraction".

In 1815, Biot (2) discovered that optical activity was exhibited by liquid terpenes; he also succeeded in proving that aqueous solutions of sucrose and tartaric acid were optically active. This led him to believe that optical activity is a property of microscopic units of matter and not only of crystalline structures. It is a well-known fact that Biot was correct in both of his views regarding the occurrence of optical activity. Another milestone in the field was set by crystallographer Louis Pasteur. He hand-sorted crystals of sodium ammonium racemate into two enantiomorphous types with opposite optical activity. Pasteur extended his work to tartrates and introduced the concept of " molecular dissymmetry ". He concluded that optically active substances should exist in two different forms which are non-superimposable mirror images of each other. The enantiomers rotate the light equally but in opposite directions. When the number of molecules of one rotation exceed those of the opposite rotation, a net optical activity

results, but a 1:1 mixture should be optically inactive (racemic).

In 1874 Van't Hoff and Le Bel independently but simultaneously related organic structures with optical activity. They rationalized the known cases of optical isomers containing an asymmetrically substituted carbon atom in terms of a tetrahedral array of the carbon valencies. Werner later resolved a purely inorganic trischelate complex (1914) and disposed of the assumption that organic carbon is the essential constituent of optical activity.

B. Introduction to chiroptical techniques

Chirality can be defined as the non-congruence of an object and its mirror image. The property of chirality is an interesting aspect of molecular stereochemistry. Common spectroscopic methods utilized in structural studies, such as NMR and IR spectroscopies etc., and methods based on the physical properties like density, melting point, molecular weight etc., cannot probe the chirality of molecules. Any study of optically active molecules necessarily either involves other molecules which are chiral, or light, which is sensitive to handedness, viz. circularly polarized light, which interacts differentially with chiral molecules. The most familiar manifestations of these interactions are optical rotation, (or optical rotatory dispersion when measured as a function of wavelength) and circular dichroism. Before details of these two techniques are

presented a few definitions of terms are appropriate.

Electromagnetic radiation has been proven to be a transverse wave, i.e.,the electric vector is perpendicular to the direction of propagation of light. In plane polarized light the electric vector changes in magnitude with time while its direction remains constant. In circularly polarized light it is the direction of the electric vector which changes. The magnitude of the electric vector remains constant on this case, and the tip of the electric vector traces a left or right handed helix.

All polarization states of light can be described by the interference of at least two waves, the electric vectors of which are mutually perpendicular. If the waves have the same frequency, different phase shifts can be shown (3) to produce different polarizations of light. A phase difference of 0 or multiples of π will give plane polarized light. In a special case, when the amplitudes of the two components are equal and δ ,the phase difference is odd multiples of $\pi/2$, the vibration formed is a circle and the light is said to be circularly polarized (Fig.1).

To exhibit optical activity, molecules have to be chiral and both the enantiomers must be separated. The sufficient and necessary condition for chirality is dissymmetry (C_n, D_n). Dissymmetric molecules may have pure rotation axis but not any other element of symmetry such as center of symmetry or reflection axis. A typical example is given in Fig.2b. Most optically active molecules, however, lack

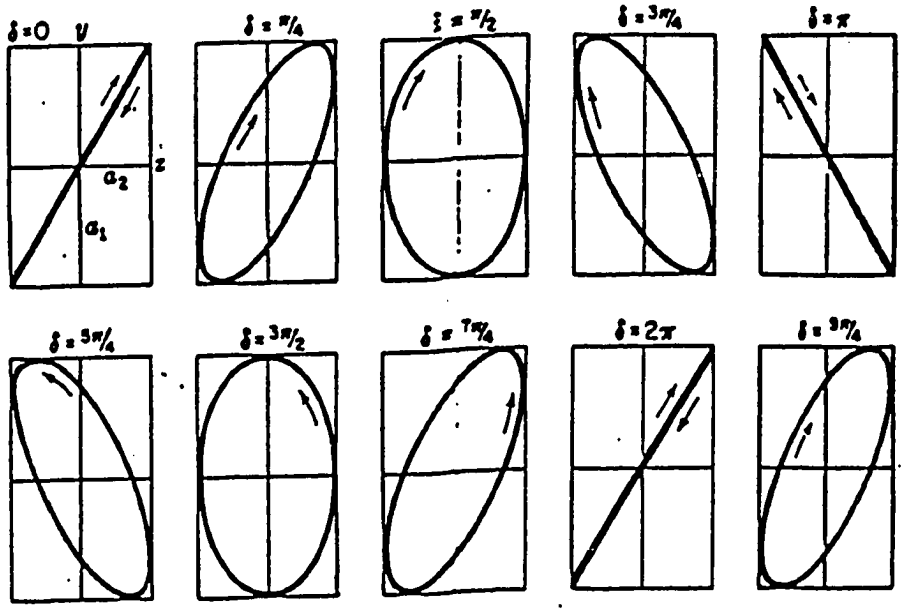

Composition at right angles of two simple harmonic motions of the same frequency but different phase.

Figure 1. Circularly polarized light.
(From Reference 3).

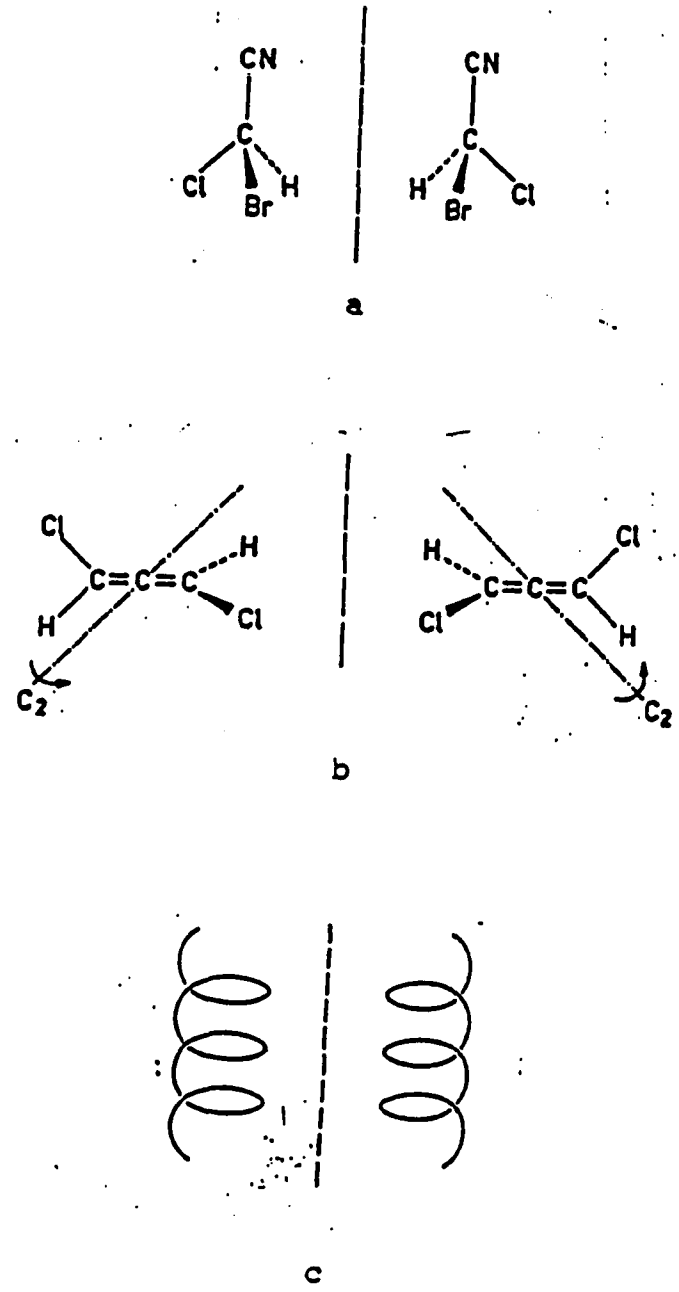

Figure 2. Examples of chiral molecules.
(From Reference 4).

any element of symmetry and may be properly called asymmetric. Bromochlorocyanomethane is a good example (Fig.2a). A helical array of atoms or groups of atoms is chiral since left and right handed helices are mirror images of each other. Large biomolecules, such as proteins, poly-saccharides and DNA may have helical structures (Fig.2c).

C. Electronic optical activity (ORD and CD)

One manifestation of optical activity is optical rotation, i.e. the rotation of plane of polarization of light passing through an optically active medium. A polarimeter is used to measure the angle of rotation. The rotation exhibited by an optically active substance depends on the thickness of the path traversed by light, the wavelength of light used and the temperature (5).

For solutions, concentration is an additional factor. The specific rotation frequently used is defined by [α]:

$$[\alpha] = \alpha\, 100/bC \qquad \text{(II.1)}$$

where α is the observed rotation in degrees, b is the layer thickness in decimeters and C is the concentration of solute (in grams per 100 mL of solution). The standard wavelength used is the sodium doublet (589/589.6 nm) and the standard temperature is 20^{o}C.

A combination of a polarimeter with a monochromater is used to measure optical rotation at various wavelengths and subsequently obtain a optical rotatory dispersion curve. Optical rotation is related to the differences in the

refractive indices of the medium for left and right circularly polarized light as follows:

$$[\Phi] = \pi/\lambda\ (n_L - n_R) \qquad \text{(II.2)}$$

where Φ, the molecular rotation is defined as

$$\Phi = [\alpha] \times MW / 100 \qquad \text{(II.3)}$$

In the above equation, n refers to the refractive index of the medium and MW is the gram molecular weight of the sample. Cotton (6) discovered an interesting relationship between rotatory power and light absorption in optically active compounds. For a compound devoid of chromophores, the optical activity progressively decreases as the wavelength increases. A plain positive or negative ORD curve is obtained. For a compound exhibiting one or more absorption bands, the behaviour is best depicted by the Drude equation (5):

$$n(\lambda) = c / (\lambda^2 - \lambda_o^2) \qquad \text{(II.4)}$$

where λ_o is the wavelength of nearest UV absorption. The rotatory power increases in the vicinity of an absorption peak but experiences a zero crossing at the peak maximum. This effect is known as the Cotton effect. Within the absorption band, the molar absorptivity for right and left circularly polarized light is different; that is

$$(\varepsilon_R - \varepsilon_L) \neq 0 \qquad \text{(II.5)}$$

As a result of this, linearly polarized light is changed into elliptically polarized light and the phenomenon is called circular dichroism or CD. Only molecules possessing accessible electronic transitions give rise to absorption

and hence CD. If $\varepsilon_L > \varepsilon_R$, then the R component of the electric vector will have a larger amplitude than the L component. Furthermore if $n_R > n_L$, then the R component will be retarded more than the L component. The resulting elliptically polarized light is shown in Fig.3.

CD can be measured using a circular dichrograph, which consists of an absorption spectrometer to which provisions to produce circularly polarized light have been added. Typically, modulators like Pockel cells are employed for this purpose (vide infra). After passing through the sample, both the alternating and DC components of the light are measured using appropriate detectors and amplifiers. More details can be found in Ref.7.

A typical example of Cotton effect is illustrated in Fig.4. In the example there are two chromophores absorbing above 200nm. The transition at 293 nm is optically active and shows a positive Cotton effect. The maxima of CD and absorption and the inflection of the ORD curve coincide in wavelength. The behaviour of the dispersion curve outside the absorption band is observed as expected (vide supra).

ORD and CD have made great impacts on modern science. These cover strucural and stereochemical problems in organic chemistry, conformational problems in biochemistry (eg., the helicity of protein chains) and steric aspects of inorganic and organo-metallic compounds. Specific empirical rules, such as the octant rule, sector rule and quadrant rule, are established to correlate configuration and

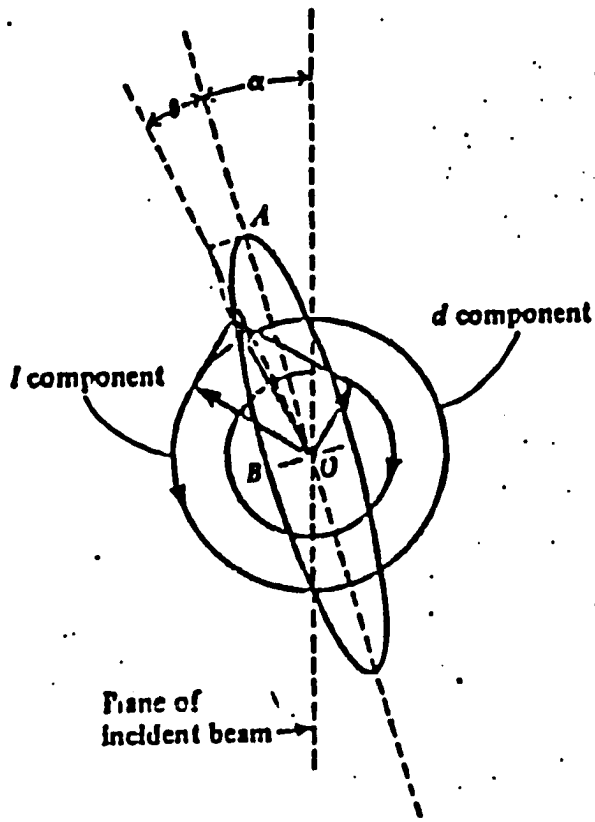

Elliptically polarized light produced when $\eta_d > \eta_l$ and $\epsilon_l > \epsilon_d$.

Figure 3. Elliptically polarized light.

(From Reference 5).

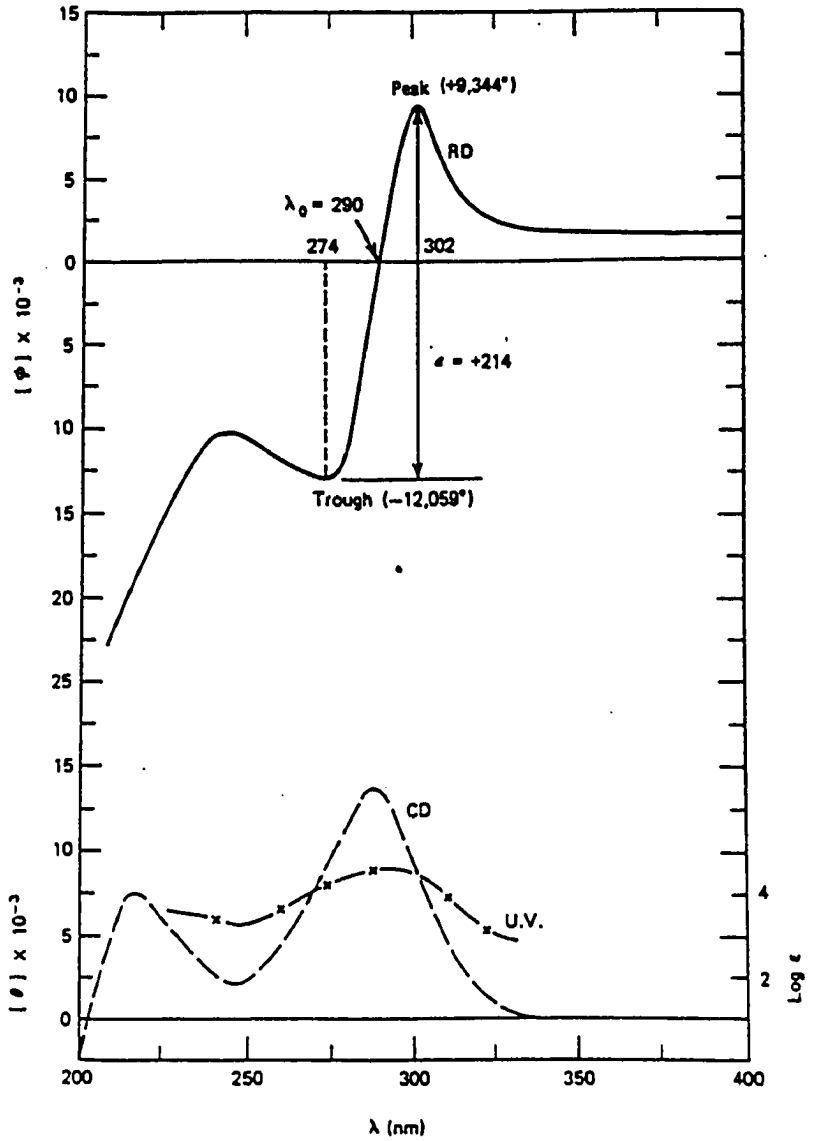

Fig. 3.10. RD, CD, and U.V. curves of *N*-(5,5-dimethyl-2-cyclohexen-1-on-3-yl)-gitingensine (2).

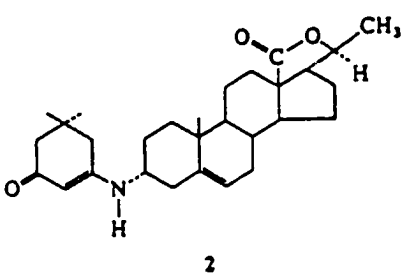

2

Figure 4. Cotton effect (From Reference 7).

conformation with the sign and intensity of Cotton effects exhibited by chromophores. The "octant" rule emerged out of studies on steroids by Djerassi and his coworkers. It expresses the relationship between the absolute configuration of the perturbing environment, and the sign and the intensity of the Cotton effect associated with the carbonyl $n \rightarrow \pi^*$ transition (more details can be found in Ref.8). The rule has been successfully applied to aliphatic optically active ketones and aldehydes and to mono- and poly cyclic keto derivatives. Modifications of the octant rule have been proposed for the $n \rightarrow \pi^*$ band of β-unsaturated ketones. The work of Klyne and his collaborators with lactones gave the lactone sector rule (8). This rule is based on the assumption that the lactone (cyclic ester) group may be considered to be roughly planar and suggests that the space around the lactone group may be divided into sectors by means of planes meeting at the carboxyl carbon atom.

New correlation studies have been made for aromatic chromophores, nucleotides and nucleosides in the last decade. More progress in the instrumental techniques and theoretical interpretations are in the way.

D. Vibrational optical activity (VOA)

As discussed earlier, VOA methods are comparatively richer in stereochemical information than the electronic optical activity methods. These new spectroscopic methods

have opened new doors in the field of conformational and vibrational studies of small molecules, polymers and metal complexes. Although VCD and ROA both deal with vibrational transitions, the origin of the effects are entirely different and they provide complementary structural information. In the following section, VCD and ROA will be considered separately and their different features will be discussed in an appropriate fashion.

1. Vibrational circular dichroism (VCD)

a. Instrumental

Vibrational circular dichroism, the differential absorption of circularly polarized infrared light by chiral molecules, was first reported by George Holzworth and co-workers at the University of Chicago in 1973 for crystals (9) and 1974 for neat liquids (10). Since then, VCD has made great progress theoretically and experimentally. VCD has been successfully applied to the studies of a wide range of molecules like peptides, sugars, amino-acids, polymers and, most recently, nucleotides. An extensive review of the most recent stereochemical applications of VCD can be found in Ref. 11.

VCD signals are at least four orders of magnitude smaller than the parent IR intensities. To overcome the noise and other short-term instabilities, the VCD is observed via a high frequency modulation experiment. The incident light is modulated between left and right polarization via a

photo-elastic modulator(PEM). The PEM produces circularly polarized light via stress birefringence (12). The desired VCD signal is contained in an AC signal at the frequency of the PEM.

The first generation VCD instruments were dispersive systems, the wavenumber range of which was restricted to the frequency region above 2000 cm^{-1} due to detector limitations. Second generation instruments have extended the spectral coverage through the mid IR region to 600 cm^{-1}. VCD can also be observed via Fourier Transform (FT) measurement although the advantage of FT is less in VCD than in IR spectroscopy. To date, FT-VCD measurements have spanned the frequency range from 3400-600 cm^{-1}. At Hunter college, a dispersive VCD instrument has been constructed recently, and data acquired are shown to be (13) comparable to those obtained via a FT instrument in resolution and signal to noise ratio.

b. Theoretical considerations

In a VCD experiment one obtains a spectrum of ΔA versus wavenumber. While the IR intensities are due to the change in the dipole moment during vibrations, the VCD intensities arise from the interaction of the electric dipole moment and the magnetic dipole moment. The IR intensities of a i --> j vibrational transition are proportional to the dipole strength D. i and j denote ground and excited vibrational states.

$$D_{ji} = |\mu_{ji}|^2 \qquad \text{(II.6)}$$

where μ_{ji} is the electric dipole transition moment (vide infra). The VCD intensities depend on a similar term called the rotational stregth R. The rotational strength R_{ji} is defined as,

$$R_{ji} = \text{Im}\,(\mu_{ji}) \cdot (m_{ji}) \qquad \text{(II.7)}$$

Here m refers to the magnetic dipole transition moment. The dipole and rotational strengths are related to the experimentally observed intensities by

$$g = \Delta\varepsilon/\varepsilon = 4R/D \qquad \text{(II.8)}$$

In the above equation g is the anisotropy factor and it is the measure of the chiral perturbation of a chromophore. The theoretical equations are quite analagous to those obtained for the electronic CD. The difference lies in the fact that in VCD, the electronic ground state does not change during the transition. The fact that the excitations involve only the ground electronic state makes the VCD calculations deceptively simple. However, since the electronic contribution to a vibrational magnetic dipole moment vanishes within the Born-Oppenheimer* approximation (BO), the VCD intensities are observed as a result of the breakdown of the Born-Oppenheimer approximation.

A comprehensive theoretical calculation using corrected and more accurate wavefunctions than those specified by the BO approximation was given recently by Stephens (14). Theo-

*- Born-Oppenheimer principle: The nuclear motion in ordinary molecular vibrations are so slow that they do not affect the electronic states of molecules.

retical models have been very succesful in VCD and are of great interest. The VCD models will be discussed in an elaborate fashion in a later section of this chapter.

2. Raman optical activity (ROA)

Unlike its companion technique, ROA as well as Raman spectroscopy are scattering and not absorption phenomena. Scattering is an interesting light-matter interaction. When radiation impinges on a molecule, dipoles are induced. These dipoles oscillate and form the source of scattered radiation. To a first approximation, the induced dipole moment is proportional to the electric field as:

$$\mu = \alpha E_o \cos 2\pi\nu_o t \qquad \text{(II.9)}$$

where α is the molecular polarizability, E_o the amplitude of the electric field oscillations, and ν_o the frequency of the incident radiation. The polarizability of a molecule changes during vibrational motion. For a given normal mode of frequency ν_m ,

$$\alpha = \alpha_o + \alpha_1 \cos[2\nu_m t\pi + \beta] \qquad \text{(II.10)}$$

where β is an arbitrary phase. Substitution in Eq. (11) yields

$$= \alpha_o E_o \cos 2\nu_o t\pi + \alpha_1 E_o \cos 2\pi\nu_o t \times \cos[2\pi\nu_m t + \beta] \qquad \text{(II.11)}$$

By classical electromagnetic theory , an oscillating dipole radiates power at a rate given by

$$I = (16\pi^4 \nu^4 / 3c^3)\ (\mu)^2 \qquad \text{(II.12)}$$

Substituting in the above equation the previous expression for μ one gets,

$$I = 16\pi^4\nu^4/\ 3c^3[\alpha_o^2 E^2\cos^2 2\pi\nu_o t + \alpha_o E^2\cos^2 2\pi(\nu_o+\nu_m)t + \beta_o + \alpha_o E^2\cos^2[2\pi(\nu_o-\nu_m)t - \beta] + \text{cross terms}] \quad (II.13)$$

The first term corresponds to scattering without change in frequency and in phase with the incident light, i.e., coherent Rayleigh scattering and the second and third terms correspond to scattering with change of frequency or Raman scattering. Thus while the equillibrium polarizabilty gives rise to Rayleigh scattering, it is the change of polarizability during a vibrational motion which is responsible for the Raman effect (15). The frequencies are shifted from the original Rayleigh line and the shift in frequencies correspond to vibrational frequencies characteristic of the molecule. With the advent of powerful laser sources and efficient photodetectors, the Raman effect enjoys a prominent position in vibrational spectroscopy at present. It provides information complementary to IR data and is widely used as a routine analytical tool.

In the late sixties, when the theory of VCD was formulated and prediction about the VCD intensities were made, chemists in the field felt that, it was timely to exploit the possiblity of ROA. The fundamental scattering mechanisms responsible for ROA was formulated by Atkins and Barron in 1969 (16). They considered the interaction between the molecular polarizability tensors (vide infra) and the optical activity tensors in optically active molecules. The scattered light intensity was found to depend on the degree of circular polarization of the incident light.

Barron and Buckingham subsequently developed the theory and introduced the dimensionless circular intensity differential CID or Δ (17). The first genuine ROA was reported by Barron and co-workers in 1973 (18).

In the beginning years, ROA data were collected using Raman instruments to which modulation optics were added. Experimental progress in ROA has been rather slow for several reasons (vide infra). The use of a multichannel detection system brought in a whole new advantage for the field (more details will be given in a later chapter). It was discovered that the effect is not only small but is accompanied by strong artefacts which can entirely mask ROA. Sources for these artefacts were determined and solutions suggested (19,20). The experiment involves very subtle optics alignments for which systematic procedures have been cited (21). At this moment, it seems that most of the obstacles in the way of collecting reliable ROA data have been completely addressed. As in ordinary Raman spectroscopy, two independent polarization measurements can be done in ROA (using an analyser placed perpendicular and parallel to the laser polarization plane). It is strongly hoped, that the stereochemical informations obtained from the ROA experiment will be more than just worthwhile.

E. Magnetic vibrational optical activity

All molecules in a magnetic field can exhibit ORD and CD (the Faraday effct). Manifestiations of the same have

been found in VCD (22) and in ROA (23). These effects involve achiral molecules but are found to provide enormous information regarding the magnetic structues of energy levels. However, this topic will not be discussed further in this thesis.

III. THEORETICAL CONSIDERATIONS

A. Introduction

It has been mentioned frequently in the preceeding sections of this thesis that optically active molecules respond in a different fashion to left and circularly polarized radiation. It is now in order to explore the origin of these "differential interactions". In 1928, Rosenfeld gave the quantum mechanical treatment for the phenomenon of optical activity. His theory can be extended with ease to include VCD and modified to accomodate ROA. However, in all the cases, approximate wavefunctions are utilized, and so comparison of theory and experiment has not been quite fruitful. For this reason, empirical rules are established along with the development of theoretical models in few cases. An inquiry into the models in the field is therefore an integral part of the theoretical review and will be taken up after the discussion of the theory. Symmetry rules based on group theory will provide additional room for clarity and are aptly included in this chapter.

B. Theory of natural optical activity

When light passes through any medium, it undergoes two changes: the intensity of light is reduced because of absorption and the speed of light changes as it traverses along the medium. Beer's law of absorption requires that

$$I = I_0 \, e^{(-4\pi\varepsilon/\lambda)l} \qquad \text{(III.1)}$$

where I_0 is the initial intensity of a beam of wavelength λ impinging on a medium whose absorption coefficient is ε and I is its intensity after it has travelled through a distance l in the medium.

The index of refraction or refractive index n of any optical medium n is defined as the ratio between the speed of light in vacuum c, and the speed of light v in the medium v.

$$n = c/v \qquad \text{(III.2)}$$

The behaviour of light incident on the boundary between two different media is governed by the laws of reflection and refraction. The angle of incidence is equal to the angle of reflection as per the law of reflection. According to the law of refraction,

$$\sin \Phi_i / \sin \Phi_r = n_{21} \qquad \text{(III.3)}$$

where Φ_i and Φ_r are the angles of reflection and refraction respectively and n_{21} is the relative index defined by $n_{21} = n_2/n_1$.

The subject of dispersion concerns the refractive index of substances and its variation with wavelength. Generally the refractive index decreases with increase in wavelength. However, in the neighbourhood of an absorption band, the longer wavelengths have higher refractive indices and are more refracted (anamolous dispersion). Drude gave the equation to accomodate the phenomenon of dispersion and the anamalous dispersion (vide supra).

As noted earlier, optical rotatory dispersion (ORD) and

circular dichroism (CD) are due to the fact that chiral molecules have different refractive indices for left and right circularly polarized light ($n_R \neq n_L$) and their absorption coefficents for both polarizations are unequal ($\varepsilon_R \neq \varepsilon_L$). The theory of optical activity attempts to unfold the reason for this, by investigating the nature of the interaction of chiral molecules with elctromagnetic radiation.

Electromagnetic radiation is composed of two oscillating components - electric and magnetic fields. The two vectors are both perpendicular to the direction of propagation of light (say, the z-axis along $\tilde{k}$). The electric field associated with the light wave at any time t can be expressed as

$$E = \tilde{i}\, E_0 \cos 2\pi\nu (t-z/c) \qquad \text{(III.4)}$$

where E_0 is a vector whose size and direction are constant in both time and space, c is the velocity of light and ν, the frequency. The magnetic field, H at any point in a light wave, is equal in magnitude to E, provided that E is expressed in electrostatic units (e.s.u.) and H in electromagnetic units (e.m.u.) and is given by

$$H = \tilde{j}\, E_0 \cos 2\pi\nu (t-z/c) \qquad \text{(III.5)}$$

However E and H differ in their directions in such a way that E,H and z form a right-handed system (Fig.5).

As a result of matter-light interaction, dipoles are induced in the molecule. These dipoles oscillate and form the source of the scattered radiation and account for any

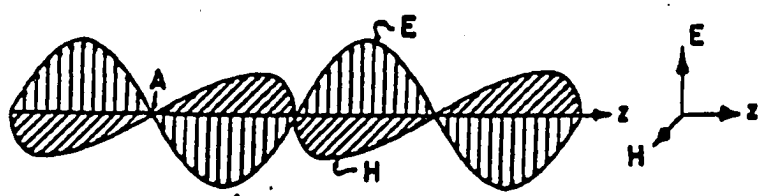

The structure of a light wave moving toward the right. Note that when the electric field, *E*, is pointing toward the top of the page, the magnetic field, *H*, points out of the plane of the paper toward the reader.

Figure 5. (From Reference 24).

other changes the light beam encounters. The electric dipole moment induced in a molecule can be given as

$$P_\alpha = \alpha_{\alpha\beta} E_\beta \qquad \text{(III.6)}$$

where $\alpha_{\alpha\beta}$ is called the polarizability tensor. The subscripts denote summation over all cartesian components:

$$P_x = \alpha_{xx} E_x + \alpha_{xy} E_y + \alpha_{xz} E_z \qquad \text{(III.7)}$$

The magnetic field induced is given by a similar expression as

$$M = \beta_{\alpha\beta} H_\beta \qquad \text{(III.8)}$$

where $\beta_{\alpha\beta}$ is called the magnetic polarizability tensor.

All the above equations can be converted into the expressions involving the corresponding macroscopic quantities by assuming that the effective local field is the same as that of the light wave. The transformation then simply involves a substitution given below:

$$(1+4\pi N_1 \alpha) = \varepsilon \qquad \text{(III.9)}$$

where N_1 is the number of molecules in unit volume and ε is is the dielectric constant of the medium. Solving Maxwell's equations using (III.6,8 and 9) will give the relation between n and ε as (25)

$$n = \varepsilon^{1/2} \qquad \text{(III.10)}$$

Rosenfeld observed that optical activity can only be explained when the higher order contributions such as the the time variation of the magnetic field, dH/dt and the electric field gradient, dE/dx were included in the expressions for the dipole moments. The modified Rosenfeld's equations for the dipole moments are given below:

$$P_\alpha = \alpha_{\alpha\beta} E - \beta_{\alpha\beta} (d/dt) H \qquad \text{(III.11)}$$

$$M = H_\beta - \beta_{\alpha\beta} (d/dt) E \qquad \text{(III.12)}$$

In the above equations $\beta_{\alpha\beta}$ is an interaction term between electric and magnetic transition moments known as the "rotatory polarizability". In optically inactive media, these additional contributions average out to zero. Solving Maxwell's equations using (III.11) and (III.12) gives,

$$n_R = \varepsilon^{1/2} - 2\pi\gamma\beta \qquad \text{(III.13)}$$

$$n_L = \varepsilon^{1/2} + 2\pi\gamma\beta \qquad \text{(III.14)}$$

From (III.13) and (III.14) it follows that

$$[\Phi] = (\pi/\lambda)(n_L - n_R) = (4\pi c/\lambda)\beta_{\alpha\beta} \qquad \text{(III.15)}$$

Thus the molecular rotation can be directly related to the molecular quantities α and β (25).

A quantum mechanical expression for the polarizability tensor can be obtained using time-independent perturbation theory: (26)

$$\alpha_{\alpha\beta} = [2/3h] \Sigma w_{ij} [(w_{ij} - w^2)^{-1}] \langle i|\mu_\alpha|j\rangle \cdot \langle j|\mu_\beta|i\rangle \qquad \text{(III.16)}$$

In the above equation i and j are molecular electronic states, w_{ij} is the transition frequency between the two states, h is the Plank's constant and μ_α is the dipole moment operator, given by,

$$\mu_\alpha = \Sigma\ e_i\ r_i \qquad \text{(III.17)}$$

where e_i denotes the charge on the particle and r_i is its cartesian position vector. The summation is over all the particles of the molecule. In a similar manner, the rotatory polarizability tensor β can be shown to be

$$\beta_{\alpha\beta} = [c/3h]\Sigma [w_{ij} (w_{ij} - w^2)] \text{ Im } \langle i|\mu|j\rangle.\langle j|m|i\rangle \quad \text{(III.18)}$$

Here, m is the magnetic dipole moment operator :

$$m = \Sigma (e_i/2m_i)\ r_i\, \varepsilon_{\alpha\beta\gamma} P_i = \Sigma e_i/2m_i\ (r_i \times P_i) \quad \text{(III.19)}$$

where m_i is the mass of the particle and P_i is its momentum; $\varepsilon_{\alpha\beta\gamma}$ is a unitary antisymmetric tensor. Handedness is inherent in the definition of the magnetic dipole moment operator which is a cross product of two vectors. Thus, the quantum mechanical approach agrees with the classical idea that the term involving electric dipole and magnetic dipole interaction is sensitive to handedness and gives rise to differential interaction of optically active molecules with circularly polarized light.

It is seen from equation (III.18), that β, the rotatory polarizability tensor is a summation over all products of electric and magnetic transition moments. A better alternative is the quantity called rotational strength R_{ij}.

R_{ij} is defined as

$$R_{ij} = \text{Im } \Sigma \langle i|\mu|j\rangle.\langle j|m|i\rangle \quad \text{(III.20)}$$

Using the equation (III.20), one can estimate the contribution to the observed optical activity for a particular transition (26). R and β are related as follows:

$$\beta = [c/3h]\Sigma R_{ij}\ W_{ij}\ /(w_{ij} - w^2) \quad \text{(III.21)}$$

R_{ij} is quite analogous to the dipole strength in electronic absorption spectroscopy:

$$D_{ij} = \langle i|\mu|j\rangle^2 = \int_{\text{band}} \frac{\varepsilon}{\nu}\, d\nu \quad \text{(III.22a)}$$

The intensity of a CD band is proportional to the quantity R_{ij}:

$$R_{ij} = \text{Im} \langle i|\mu|j\rangle \cdot \langle j|m|i\rangle = \int_{\text{band}} \frac{\Delta\varepsilon}{\nu} d\nu \qquad \text{(III.22b)}$$

C. Theory of ROA:

It has been pointed out above that the induced multipoles are responsible for the scattering of radiation. In the expression for the induced electric dipole, the contribution from the field gradient E has to be included along with that from the time variant of the magnetic field. For ORD and CD, the contribution due to electric quadrupole cancels out (26). For Rayleigh and Raman scattering, however, this is not true and the quadrupole contributions have to be included for the theory of ROA. The induced dipole moment in this case is given by,

$$P_\alpha = \alpha_{\alpha\beta} E_\beta - G_{\alpha\beta}(d/dt)\, H + 1/3\, A_{\alpha\gamma\beta}(\Delta_\beta E_\gamma) \qquad \text{(III.23)}$$

The above equation is similar to (III.11) but for G replacing and the additional term involving the quadrapole contribution. G and β are related as follows:

$$G_{\alpha\beta} = \Sigma i w\, 3/c\, \beta_{\alpha\beta} \qquad \text{(III.24)}$$

$A_{\alpha\beta\gamma}$ is the three dimensional field gradient tensor defined by:

$$A_{\alpha\beta\gamma} = [2/h]\Sigma w_{ij}(w_{ij} - w^2)^{-1} \langle i|\mu_\alpha|j\rangle \cdot \langle j|\Theta_{\beta\gamma}|i\rangle \qquad \text{(III.25)}$$

where $\Theta_{\beta\gamma}$ is the electric quadrupole operator

$$2\Theta_{\alpha\beta} = \Sigma e_i(3r_{i\alpha} r_{i\beta} - r_i \delta_{\alpha\beta}) \qquad \text{(III.26)}$$

where r and e have same meaning as in equations (III.17)

and (III.19), and

$$\delta_{ij} = 0 \text{ for } i \neq j \text{ and } = 1 \text{ for } i=j \qquad \text{(III.27)}$$

In a similar manner, equations for the induced magnetic moments and quadrupole moments can be derived.

Scattered intensities may be derived as follows: Let the molecule be at the origin of the space fixed co-ordinate system x,y,z with the incident beam travelling along z and the beam scattered at 90° along the y-axis (Fig. 6). I_x and I_z specify the polarized and depolarized components of the scattered light. The electric field strength of the scattered light is then given by,

$$E_{\alpha} = -w^2/4\pi Ec^2 r\, f(P_{\alpha}, m_{\beta}, \Theta_{\alpha}) \qquad \text{(III.28)}$$

Expressions for the induced dipoles can be substituted in the above equation. By writing the field vectors of the incident light explicitly for right and left circular polarizetion using,

$$E^{\pm} = 2^{1/2} E_0 (x \pm iy) \qquad \text{(III.29)}$$

the intensities I_x and I_z can be calculated. The experimentally sought quantity called the circular intensity differential is then given by,

$$\Delta_z = \frac{4\,(3a_{\alpha\beta}G_{\alpha\beta} - a_{\alpha\alpha}G_{\beta\beta} - 1/3\; w_{\alpha\beta}A_{\alpha\beta\gamma})}{2c\,(3a_{\gamma\delta}a_{\gamma\delta} - a_{\gamma\gamma}a_{\delta\delta})} \qquad \text{(III.30)}$$

$$\Delta_x = \frac{2\,(7a_{\alpha\beta}G_{\alpha\beta} + a_{\alpha\alpha}G_{\beta\beta} + 1/3\; w_{\alpha\beta}A_{\alpha\beta\gamma})}{c\,(7a_{\gamma\beta}a_{\alpha\beta} + a_{\gamma\gamma}a_{\delta\delta})} \qquad \text{(III.31)}$$

During the above derivations, care is taken to average all the orientations of the molecule. Comprehensive and detailed step by step derivation of the circular intensity

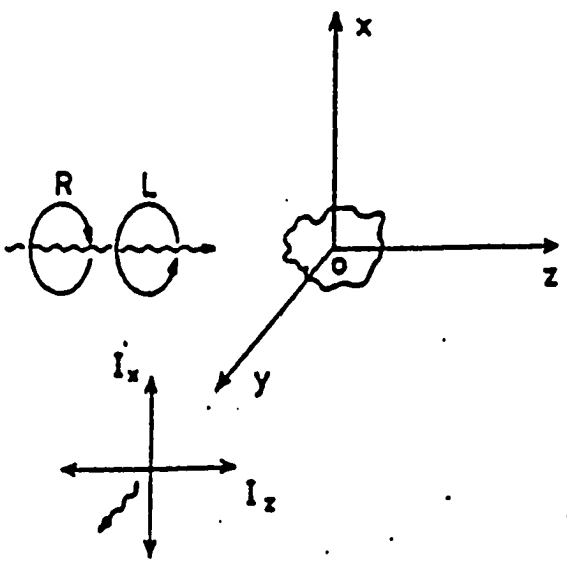

The geometry for polarized light scattering at 90°.

Figure 6. (From Reference 27).

differential (CID) can be found in several papers and reviews (27-32).

It is clear from equations (III.30, 31) that only the cross terms αG and αA contribute to the CID. Strictly speaking, the above equations apply only to Rayleigh CID. For inelastic Raman scattering, the terms of the polarizability tensor α , G are substituted by the expression $d\alpha / dQ_i$, dG / dQ_i etc., where Q_i is the i'th normal coordinate and the derivative is taken at the nuclear equillibrium position.

D. Symmetry rules in optical activity

Group theory requires that an observable has to transform like the totally symmetric representation of the point group of the molecule. In optical activity, the quantity responsible for the process is given by

$$R_{ij} = \mathrm{Im} \langle i | \mu | j \rangle \, . \, \langle j | m | i \rangle \qquad \text{(III.33)}$$

where R_{ij} is called the rotational strength (vide supra). $\mu . m$ must transform according to the scalar representation of the point group of the molecule for it to show optical rotation. The operator μ is a polar vector while m, which is (r x p), is an axial vector. The product of an axial and polar vector (μ . m) is called a pseudoscalar. In pure rotational groups, polar vectors like μ and axial vectors such as m are not differentiated by proper rotations. The result of this is that the dot product of μ and m belong to the identity or scalar representation. Thus,

these groups are allowed by group theory to exhibit optical activity. C_n, D_n, $\overline{T}$, and O are some of the few rotational groups of molecular importance. Strictly speaking, the above principle applies to molecules containing inherently asymmetric chromophores.

Schellman (33) pointed out that optical activity can arise in molecules in several different ways. Two groups which are inherently symmetric can be placed in such a way to create a dissymmetric environment and give rise to optical rotation. Schellman agreed with Kirkwood in his opinion that dipole-dipole interaction can act as a strong source for the coupling mechanism (coupled-oscillator model). For effective coupling large transition moments or proximity of the two groups is required. However, the rotational strength R increases with the distance between the two groups (vide infra - equation III.35).

Schellman also studied the form of optical rotation produced in the electronic transition on a localized group by an outside perturbation (one-electron model). He proved that in such a case the perturbing function should belong to the pseudoscalar representation of the point group of the molecule. From this study emerged regional selection rules (e.g., the octant rule for ketones and quadrant rules for peptide link) which are very useful in conformational analysis. These rules are capable of predicting the sign and magnitude of Cotton effects (vide supra) in different environments.

The above rules can be extended carefully to accomadate vibrational optical activity. The symmetry requirement for a normal mode Q_a to exhibit nonzero VOA is that the corresponding components μ and m have the symmetry of the normal mode Q_a. For asymmetric molecules, all Q's fall into the A class.

From the derivations of the Raman CID equations (III.31) and (III.32), it is obvious that the interference between the scattered waves generated through the same components of α and G is the source of ROA. Consequently if a normal mode of vibration is to show CID, the same components of $\alpha_{\alpha\beta}$ and $G_{\alpha\beta}$ (or $A_{\alpha\beta\gamma}$) must span the irreducible representation of the mode in question. This happens for molecules belonging to C_n, D_n, O, T which lack improper rotation axis. In these molecules all modes which are Raman active, are active in ROA too. Barron extended Schellman's one electron theory to polarizabilty and optical activity tensors (34). In this work, he also compared the Raman and ROA intensities. He observed that it is possible for a strong Raman band to show weak ROA and vice versa.

E. Parity in ROA

The fact that optical activity experiments conserve parity and are invariant to time-reversal has been established in 1972 by Barron (35). In another work (36), he extended these arguments to ROA.

Most physical laws, especially, those of electromagne-

tism, are unchanged by space inversion. In other words, the equations governing these laws are unchanged if the co-ordinates (x,y,z) are replaced everywhere by (-x,-y,-z). The physical phenomena described by these laws are then said to conserve parity. The symmetry operation of time-reversal reverses the motions of all the physical entities in the system. If replacement of time co-ordinate (t) by (-t) everywhere in equations representing physical laws leaves those equations unchanged, the processes are said to be time-reversal invariant. If a complete experiment is subjected to space-inversion or time-inversion, the resulting experiment should be realizable. A good example of an experiment which does not conserve parity is given by the electric analogue of the Faraday effect. It is not possible to induce optical activity in a non-disymmetric molecule by applying an electric field in the direction of propagation of the light beam.

Optical activity experiments deal with interaction of matter and electromagnetic radiation. They preserve parity and are invariant to time-reversal. In ROA, the parity operation will change the sense of circularly polarized light produced, while the time-reversal will change the direction of propagation of light. Change in the sense of polarization of light will give ROA signals of opposite sign but the latter will, in no way affect the experiment. By using the enantiomer of the original sample, one can produce ROA signals of opposite sign and hence this a

feasible and realistic experiment. ROA therefore conserves parity and is time-reversal invariant.

F. Models in VOA

1. Introduction

Any process in science draws interest and attention when exciting results are produced by an experiment. But it is not until the experimental results in a known sample are satisfactorily interpreted, a successful theory has been developed, and the results for unknowns confidently predicted, that the phenomenon is accepted as being thoroughly "investigated and understood". So it was natural for chemists to inquire into the theoretical understanding of the optical activity phenomenon following its discovery. Interpretation and prediction of optical rotatory power and CD intensities were attempted. The main obstacle has been the matrices of the wavefunctions involved. The quantity

$$\langle i|\mu|j\rangle \cdot \langle j|m|i\rangle$$

needs to be evaluated ; thus wavefunctions for ground and excited electronic states are required. Only approximate wavefunctions are available and they do not suffice to calculate the intensities in an optical activity experiment.

Chemists then resorted to developing approximate models to fit sample systems. One of the most interesting theories for optical activity is the coupled-oscillator theory. This emerged as one to explore electronic CD and ORD intensities

in molecules where two achiral groups couple efficently via dipole-dipole interaction or any other mechanism to create dissymmetry; it has been extended to accomodate VCD and molded to suit ROA (vide infra). The theory has also been generalized for molecules where the coupling extends to more than two groups.

VOA spectra give two definite charateristic patterns. Many spectra are dominated by bisignate (+-) or (-+) VOA couplets, (Fig.7) or a group of bands alternating sign in a given region. The integrated intensity of a couplet is essentially zero.

There can also be monosignate VOA intensities which introduce a net positive or negative bias for a spectral region. The monosignate VCD intensities do not arise from the coupling mechanism; they occur either from the vibrations of a group located on a chiral center or due to the perturbations produced in a group adjacent to a chiral center (vide infra).

2. Models in VCD

As mentioned earlier, VCD calculations involve non-Born-Oppenheimer-approximated wavefunctions. It is not until recently (vide supra) that calculations based on exact quantum-mechanical wavefunctions have been attempted with reasonable success (14). However, many models which are within the Born-Oppenheimer approximation have been developed and found to be of substantial value. But, the

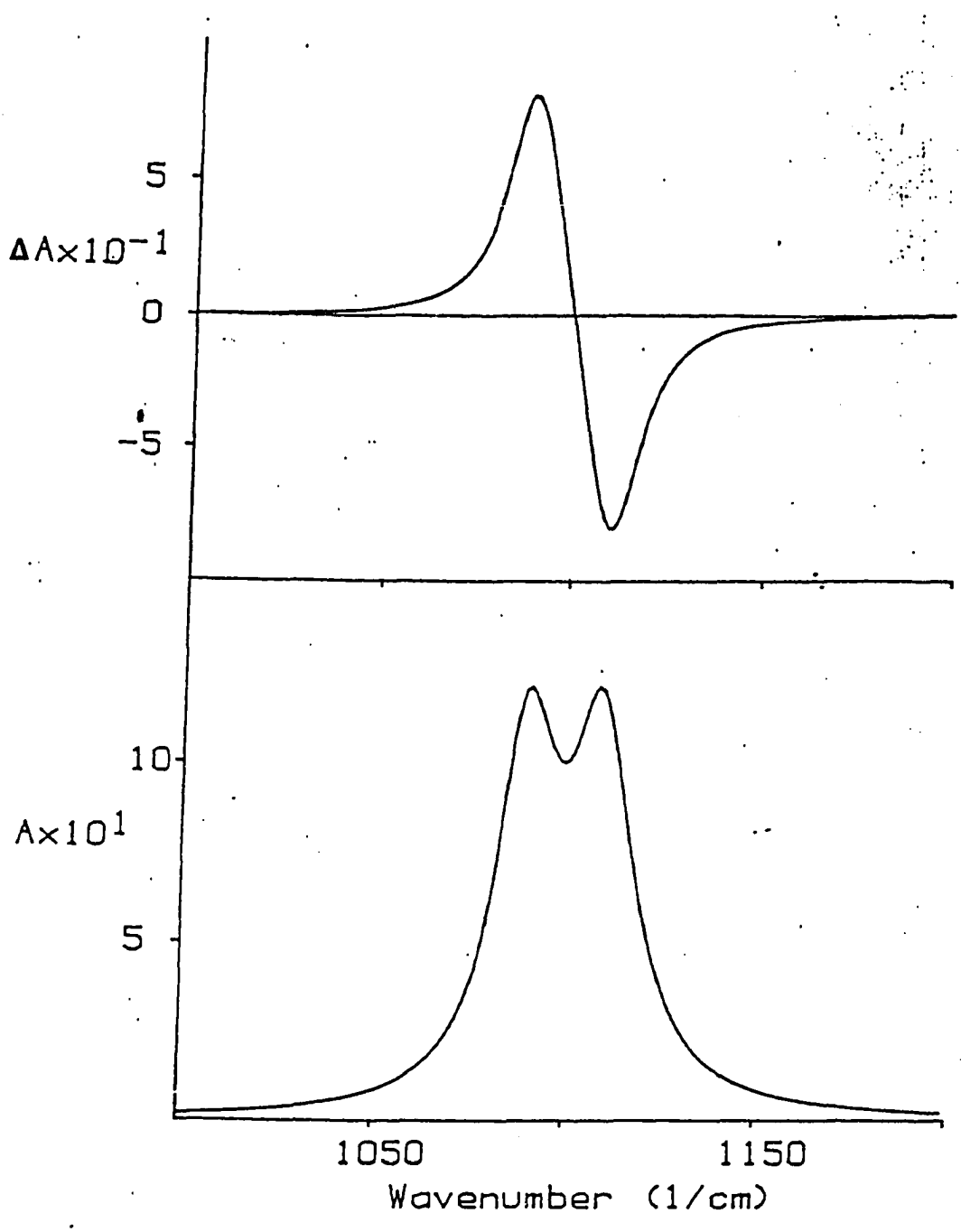

Figure 7. A typical couplet.

fact remains that each of these models is applicable only to a special group of molecules or particular type of vibrations.

The simplest mechanism for generating VCD intensities is the coupled oscillator model (37). In this theory, a vibrational perturbation mixes the motion of two local oscillators a and b with the ground state oscillator wavefunctions $\psi_a^i \psi_b^i$ and first excited wavefunctions $\psi_a^j \psi_b^j$. The coupling generates two mixed excited states:

$$\psi^{\pm} = c_1 \psi_a^i \psi_b^j \pm c_2 \psi_a^j \psi_b^i \qquad \text{(III.34)}$$

For two achiral, non-degenerate oscillators the rotational strength is then given by,

$$R^{\pm} = [w_{ab}/2c][\, T_{ab} \cdot \mu_a \times \mu_b] \qquad \text{(III.35)}$$

where w_{ab} is the average frequency of the two oscillators, λ is the mixing parameter and T_{ab} is the distance vector. The mixing parameter λ is given by

$$\lambda = \langle \psi_a^j \psi_b^i | V_{ab} | \psi_a^i \psi_b^j \rangle / (E_a - E_b) \qquad \text{(III.36)}$$

In the above equation V_{ab} is the potential energy term:

$$V_{ab} = \mu_a . \mu_b / T^3 + 3 (\mu_a . T)(\mu_b . T) / T^5 \qquad \text{(III.36 b)}$$

The interaction or the mixing of the two states generates a VCD couplet. The necessary condition is that the two groups lie in different planes in order to create dissymmetry via the coupling mechanism. The intensities and the degree of mixing depends on the energy difference between the uncoupled modes, $E_a - E_b$. Direct stereochemical information can be derived from VCD couplets using the coupled-oscillator theory (For details see Ref. 11).

There are other computational models in VCD namely the fixed partial charge (38), charge flow (11), localized molecular orbital model and the atomic polar tensor model (11). Contribution to the magnetic moment due to charge flowing around closed rings are included in the vibrational ring current model (39).

3. Models in ROA

To compute ROA intensities, "first the electronic optical activity tensors $A_{\alpha\beta\gamma}$ and $G_{\alpha\beta}$ should be given flesh and blood ", to quote Barron. Just as in other optical activity phenomena, exact wavefunctions are required to computate A and G and are unavailable. Construction of theoretical models to compute the sign and magnitude of ROA intensities in chiral molecules have been attempted. One of the models for ROA is the two-group model developed by Barron (40). In this model, Rayleigh and Raman CID's are calculated for a dissymmetric molecule containing two neutral optically inactive groups. The two groups scatter light independently and these scattered waves interfere and give rise to ROA. Here no coupling is required unlike in the case of other optically active phenomena. Differential scattering intensities increase with the distance between the two groups whereas optical rotation decreases. Barron developed a special theory called `inertia model ' for oscillations that accompany a methyl torsional vibration in molecules (41). He combined

the two group model with the inertia model and gave the bond polarizability theory (42, 43). The bond polarizability theory calculations give a very interesting and valuable result. It predicts that for axially symmetric bonds,

$$(I^R_x - I^L_x)/(I^R_z - I^L_z) = 2 \qquad \text{(III.37)}$$

where I_x and I_z are the polarized and depolarized intensities (vide supra).

Other interesting models in ROA include localized molecular orbital model and atomic polar tensor model. Prasad and Burrow have developed an atom dipole approach to ROA which provides a direct method for the calculation of ROA (44). The bond polarizability theory and the atom dipole model have been used to calculate the CID's for R(+)-chloroflurobromomethane but the predicted signs as well as intensites contradict each other. Either ROA of the molecule in question should be obtained or the theories should try more accessible molecules to acsertain as to which theory gives the best description indeed.

IV. EXPERIMENTAL

A. Introduction

The measured quantity in a ROA experiment is the dimensionless CID (circular intensity differential) :

$$\Delta = (I_R - I_L)/(I_R + I_L)$$

Here, I_R and I_L are the Raman scattered intensities for right and left circularly polarized light, respectively. ROA is capable of providing a wealth of stereochemical information and is a valuable asset to a structural chemist. Yet, the experimental progress in the field has been slow and stagnant. In principle, ROA should be a simple experiment, in which provisions to create circularly polarized light are added on to a normal Raman instrument. In practice, however, it turns out to be anything but simple. The signals sought are very small (of the order of 10^{-3}-10^{-4}) and the effect is masked by large artefacts. However, people in the field have worked their way through, with patience and endurance. Advances in the technology of the detectors and electronics have helped them capture the elusive signals while their persuasive studies of the phenomenon have shed light on the sources of the artefacts and eventually solutions to get rid of them. Now, new ROA instruments are being built in different universities and the interest in ROA is on the rise.

Owing to the small magnitude of the signals involved, it is virtually impossible to measure the scattered inten-

sities for the two polarizations separately and then determine the difference. A modulation technique has been adopted for all the chiroptical techniques since their first measurements. For ROA, it has been realized that modulation mode is highly recommended. However Barron, at a very early stage demonstrated (18) that sine wave modulation, which is employed for CD or ORD, will not work in the case of ROA because of the large polarization artefacts encountered. Thus, the first generation ROA instruments adhered to the square wave modulation of the incident light. These units were normal Raman-instruments to which light modulation optics and phase sensitive photon counting gear were added. The use of multi-channel detectors for ROA was first published by Boucher et al. (44) who demonstrated a large decrease in data acquisition times. Hug (45) constructed a ROA system with a wide spectral range, low data acquisition times and compatibility with pulsed laser sources.

B. Description of the ROA unit at Hunter college:

During the year 1983-84, a multi-channel detector equipped ROA unit was built at Hunter College. A block diagram of the instrumental set-up, as it is at present time, is given in Fig.8. The dual lens collection system which was pioneered by Hug (19) and which was shown to reduce the artefacts tremendously, is incorporated in this unit. Electronic devices and software programs for data collection and manipulation were built and developed in-house and are

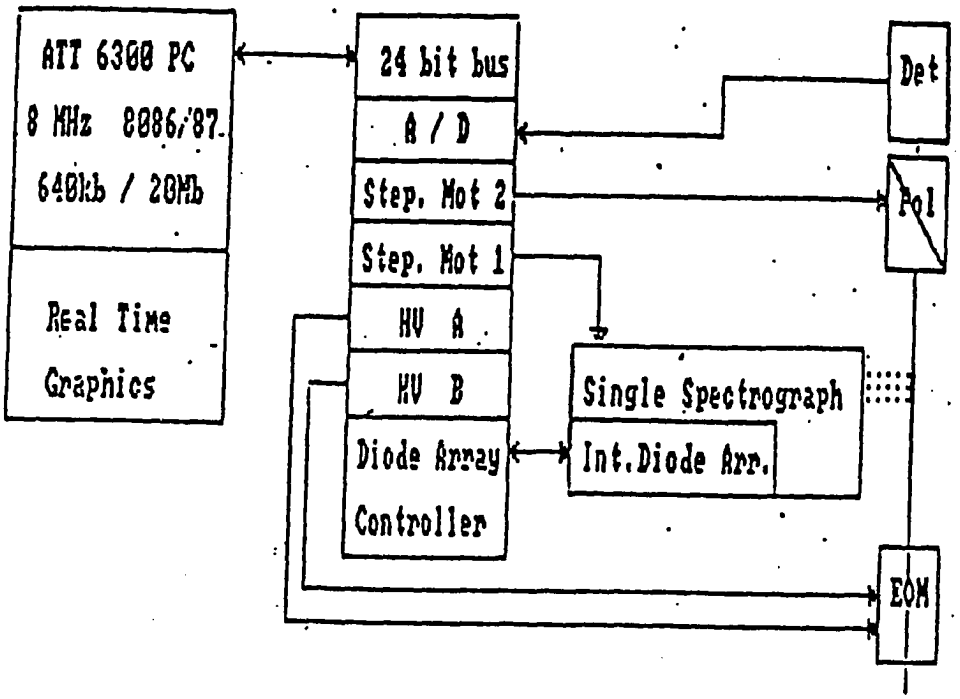

Figure 8. Electronic layout of the Hunter College Unit.

unique. The instrument has been described in detail before (21). However, since then, a few major improvements have been made. The computer system has been replaced by a AT&T 6300 personal computer featuring 8 MHZ 8086/8087 processors and 640k byte of RAM. All the software for Raman and ROA were rewritten in a powerful and sophisticated language called "Magic/L" (Loki Engineering, Cambridge, MA).

The optical lay-out of the beam optics (Fig.9) will be presented first. The beam of a Lexel Model 95-3 argon ion laser operating typically at 500 mw power at either 488 nm or 514.5 nm in light control mode, is reflected via a 45^0 mirror into a beam expander. The beam expander is made of two assymmetric lenses and gives a 3:1 expansion. It is realized from experience, that the use of a beam expander makes the alignment of EOM easier and provides less room for errors. It does so by reducing the problems associated with the inhomogeneities of the EOM (vide infra). The beam expander also reduces the possibility of local heating of the EOM crystal. The expanded beam passes through a high quality polarizer, which removes any ellipticities created by the beam expander, and is directed into the EOM (Electro-optic modulator). The EOM (Laser Metrics, Model 1057) consists of a 10mm clear aperture KD^*P (KD_2PO_4 - potassium dideuterium phosphate) crystal and is filled with index-matching liquid. The EOM is driven by a square wave corresponding to $\lambda/4$ potentials (about 1400 volts for λ = 488 nm) and produces left or right circularly polarized

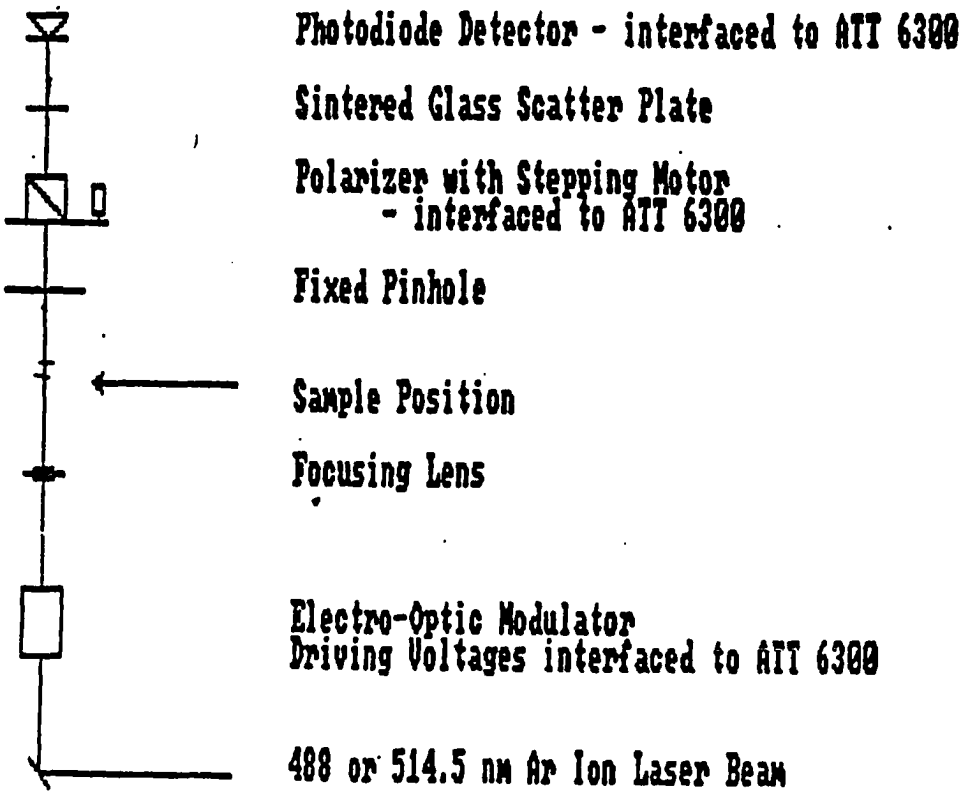

Figure 9. Measurement of beam properties.

light (see below). In spite of the anti-reflection coated windows and the index-matching fluid used, the optical transmission of the EOM is as low as 70%. This is found to be due to the actual absorption of the crystal itself. In addition to the large loss in the transmission of light, this causes a gradual heating of the optical element and necessiates temperature control of the EOM. Typically, a temperature increase of $1^{o}C$/hour may be observed without temperature stabilization of the EOM, and it has been realized that $1^{o}C$ temperature increase requires an increase in the modulation voltage of at least 5 volts. This, in turn will cause changes in the alignment conditions of the EOM and consequently, the level of artefacts will be affected (vide infra). The temperature stabilization of the EOM is one of the changes made in the instrument recently. A water-cooled copper jacket, which fits tightly around the EOM, is used. The water is kept at 21^{0} +/- $0.05^{0}C$ via a standard labaratory heating/cooling bath.

The beam from the EOM is focused into the sample cell via a 5 cm focal length achromatic lens. The cell is made of quartz with a piece of microscopic cover glass glued to its end. It is about 8 cm long with 2 mm inner diameter. In cases where samples react with glue, quartz tubes with fused ends are used. All optical components and the chuck holding the sample cell are mounted via high resolution mounts (Ardel Kinematics) on a vertical optical rail. All mounts have X and Y translational freedoms as well as

pitch, yaw and azimuth adjustments. For alignment of the EOM, the sample cell and the focusing lens can be swung out of the beam. The laser beam then passes through a second, rotatable prism polarizer and subsequently strikes a laser powermeter head, the output of which is directly read by the computer (see alignment of the EOM section). The power meter incorporates a sintered glass plate to remove any polarization sensitivity of the detector.

The power meter, rotatable polarizer etc., described above are used to measure the laser beam polarization parameters in the alignment procedure of the EOM, to be discussed in detail later.

The optical lay-out employed in the collection of the Raman scattered light will be described next.

The twin-lens optics system used for the collection of the scattered light is shown schematically in Fig. 10. There are two f/1.2 photographic lenses which are placed such that their optic axes are + or - 45^0 with respect to the YZ plane and perpendicular to each other. Collecting two cones of light symmetrically about the YZ plane was shown to reduce the artefacts drastically (18). The separate and distinct images of the two lenses are reflected via flat mirrors M1 and recombined at a common focus. The recombination optics, RO consists of two 45^0 mirrors arranged such that the upper half of the recombined image is due to one collection arm and the lower half to the other. The beam, then, is focused into the entrance slit of the monochroma-

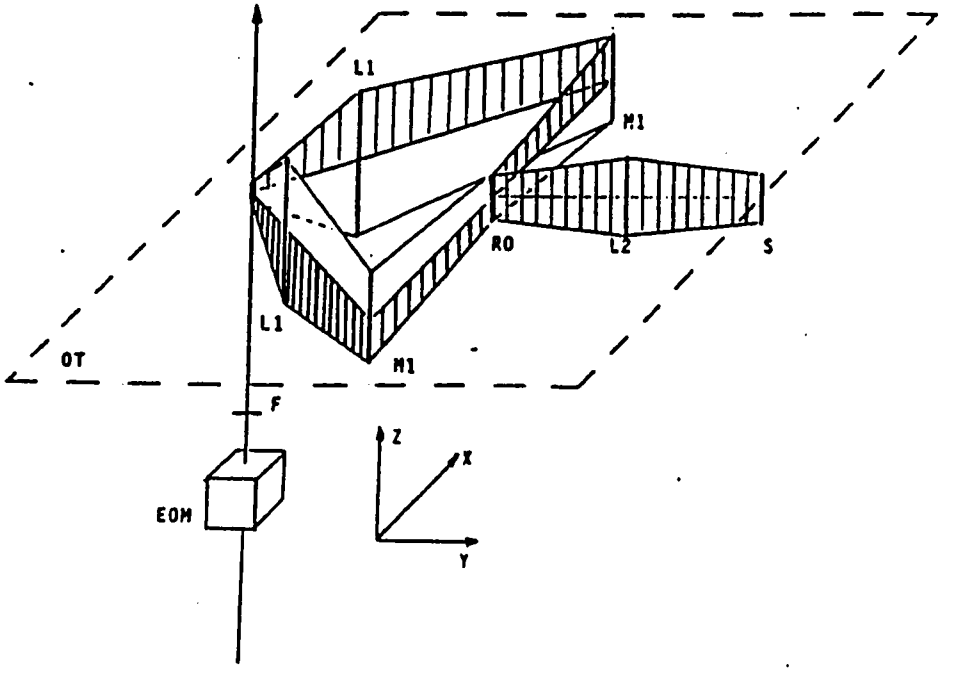

Figure 10. Dual lens collection system.

tor using a third photographic lens L2. Image magnification at the entrance slit is about 5. All reflective surfaces of the optical path are reflection enhanced, and all transparent elements have anti-reflection coatings. A sheet polarizer may be placed between the lens L2 and the slit to observe the polarized or the depolarized component of the ROA spectrum. The depolarized component has been shown to be less prone to artefacts (20) and is more commonly collected. However, the analyser drastically reduces the overall intensity reaching the spectrograph. The first total ROA data without using an analyser (vide infra) was reported in 1985 by the Hunter college group (21).

Several modifications have been made on the collection optics system in the recent past and these will be discussed now. The description of the spectrograph and the detection units will follow.

With samples exhibiting weak ROA (vide infra),it becomes crucial to maximize the total light throughput reaching the monochromator. It is also necessary to reduce any and every possible source of artefacts. The camera lenses used in the collection optics are combination systems and they might be responsible for considerable loss of valuable photons. These have also been suspected to exhibit birefringence. With the above points in mind, few changes have been made in the collection optics system in the last few months (Fig. 11). The camera lenses were replaced by fused silica lenses. These lenses, unfortunately did not meet the

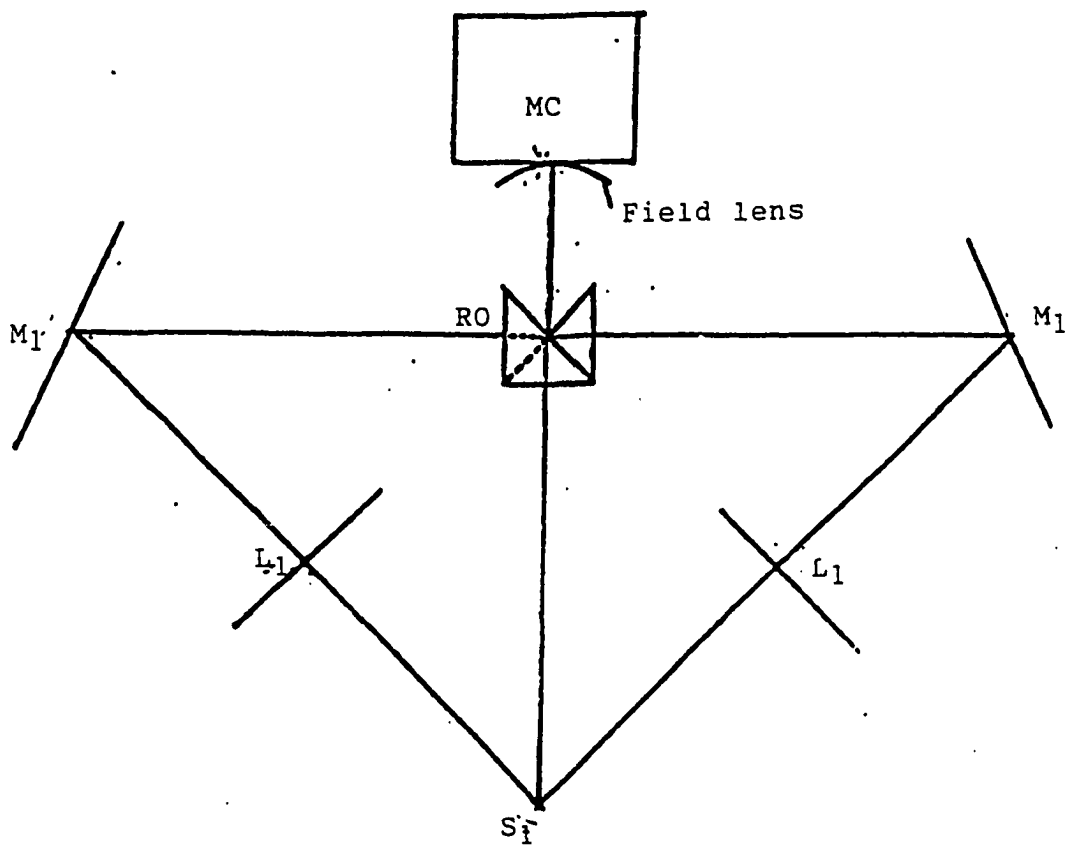

Figure 11. New collection optics layout

thin lens approximations and gave rise to high levels of aberrations and stray light problems. As a result the old camera lenses were restored in place. Also, a new recombination optics was designed consisting of two right-angled prisms whose hypotenuses have been coated with protected aluminum coating for high reflectance. The prisms have been preferred to mirrors because these are easier to mount and deform much less than mirrors in response to external mechanical stress. With coating on the hypotenuse, there is a beam path through the prism which guarantees precise right angle deflection while allowing the prism a single degree of rotational freedom. After the recombination optics, the beam is focused onto the entrance slit of the monochromator using a field lens made of glass.

In order to ensure the accuracies of the positions of different optical components on the optical table and spectrograph, a new vibration-isolated optical table has been installed. This table provides a firm, reliable, vibration-free environment isolated from external disturbances. The table structure provides internal damping to dissipate vibrations generated on the table surface. It is adequately rigid to resist bending or flexture when components are added or moved on the surface. The laser shelf and the optical table are coplanar. The position of the beam with respect to the other optical components is thus very stable. The optical table has holes drilled in which are exactly an inch apart. By choosing the appropriate holes it

has been easy as well as accurate to align the two collection arms such that they are at right angles to each other and make an angle of 45° with the laser polarization plane.

The spectrograph is a 64 cm focal length Czerny-Turner monochromator with a 100 x 100mm, 1800 grooves/mm, holographic grating. The grating may be scanned via a stepping motor under computer control such that different spectral segments of ca. 650 cm^{-1} can be examined. The image is reduced in height at the spectrograph focal plane by means of a cylindrical lens which can be rotated with high resolution in the focal plane.

The light is detected using an image-intensified, electrostatically focused diode array detector head (Tracor Northern, Model 6122) mounted kinematically on three micrometer screws at the focal plane. It consists of 1024 diodes, each 2.5 mm high and 12.5 um wide on 25 um centers. Since the diodes are well separated, there is very little blooming. Thermal shot noise in the detector can be reduced by cooling the detector to about -15°C. Consequently, the detector is purged by nitrogen or dry air to avoid the condensation of atmospheric moisture on the detector head. The procedure for the actual collection of ROA data will be taken up later in this chapter.

The alignment of the EOM, which is the first step in a ROA experiment will be described in the following section.

C. Alignment of the EOM

1. Principle of the EOM

The heart of a ROA experiment is the device producing circularly polarized light. The EOM or electro-optic modulator used by us is a Pockels cell made of a crystal of potassium dideuterium phosphate (KD^*P). On the basis of physical optics, doubly refracting crystals are classified as either uniaxial or biaxial. In uniaxial crystals, the refractive indices and hence the velocity of the ordinary and extra-ordinary (O and E) waves are equal along a unique direction called the optic axis. When some uniaxial crystals with no center of symmetry such as ADP (Ammonium dihydrogen phosphate), KDP (Potassium dihydrogen phosphate) or KD^*P are subjected to an electric field in the direction of the optic axis, polarized light travelling along this axis will be retarded; the induced birefringence depends on the wavelength λ and the applied voltage (Fig. 12). This phenomenon is called longitudional Pockels electro-optic effect. The difference in refractive indices, $n_x - n_y$, is given by

$$n_x - n_y = n^3 r_{eo} V_z / d \qquad \text{IV.1}$$

where n's are refractive indices, r_{eo} is the electro-optic coefficient, V_z is the applied voltage and d is the thickness (7). The retardation δ is then

$$\delta = (n_x - n_y)\, 2\pi d/\lambda \qquad \text{IV.2}$$

$$= 2\pi n^3 r_{eo} V_z/\lambda \qquad \text{IV.3}$$

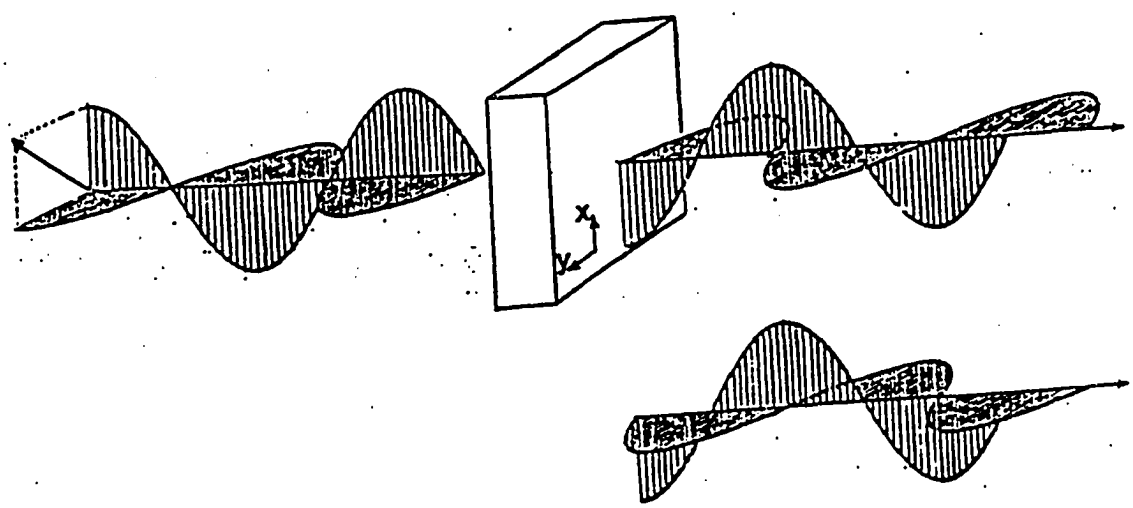

$n_x \neq n_y$ due to stress or electric field applied to crystal

Figure 12. Birefringence and circularly polarized light.

For a given wavelength the retardation is directly proportional to the electric field and is independent of the thickness. Because of the possibility of using an alternating applied voltage, the Pockel effect retarder can be used as a modulator to produce alternating right and left circularly polarized light.

The voltages can also be applied perpendicular to the optic axis (transverse Pockels effect). Although smaller electrical fields could produce circularly polarized light this way, the quality of circularly polarized light is not good. Hence the longitudional effect is preferred and employed by us.

The EOM has a few disadvantages. The parallelity of the beam and the optic axis is very crucial; even an obliquity of the magnitude of fractions of minutes can produce significant artefacts in a ROA experiment. Substantial errors in retardation can arise and there is good possibility of beam diffraction (see below). The EOM is very sensitive to alignment because of its narrow acceptance angle. It has to be operated at a constant temperature (vide supra). Suitable voltages (about $\pm$ 1400 volts for λ = 488 nm) can be selected to produce exactly $\pm \lambda/4$ retardation or left and right circularly polarized light. However, if the crystal exhibits any static birefringence, then the voltages for the right and left polarities may not be equal (vide infra).

2. Artefacts in ROA

In addition to the signals being weak, the ROA effect is plagued by artefacts. These are spurious signals which are of similar or larger magnitude than the true ROA signals. Realizing the importance of understanding these artefacts, Hug (19) and Barron and Vrbanchich (20) studied the possible sources of the artefacts extensively. The major artefacts have been proved to emerge from the device producing circularly polarized light via residual ellipticities and rotation of the polarization ellipse (see below). In Ref.20, artificial intensity differences ($W^R - W^L$) are presented by the following equations:

$$W_x^R - W_x^L = R^2 kc\,(1/\rho - 1)\,\{P_R \cos 2\eta_R \cos 2\theta_R - P_L \cos 2\eta_L \cos 2\theta_L\} \sin\Delta\alpha \sin\Delta\varepsilon/2 \qquad \text{IV.4}$$

$$W_z^R - W_z^L = -1/3\; R^2 kc\,(1/\rho - 1)\,\{P_R \cos 2\eta_R \cos 2\theta_R - P_L \cos 2\eta_L \cos 2\theta_L\} \sin\Delta\alpha \sin^3\Delta\varepsilon/2 \qquad \text{IV.5}$$

In the above equations, W_x and W_z represent the radiant energy collected per unit time through an analyzer with its axis perpendicular and parallel to the scattering plane yz respectively. P refers to the degree of polarization, which varies between zero for a completely unpolarized beam and one for a completely polarized beam; the azimuth θ is the angle between the major axis of the polarization ellipse and the x-axis (Fig. 13); and the ellipticity η of the polarization ellipse, which varies between $+\pi/4$ for right circular polarization, 0 for linear polarization and $-\pi/4$ for left circular polarization. η is the ellipticity defined

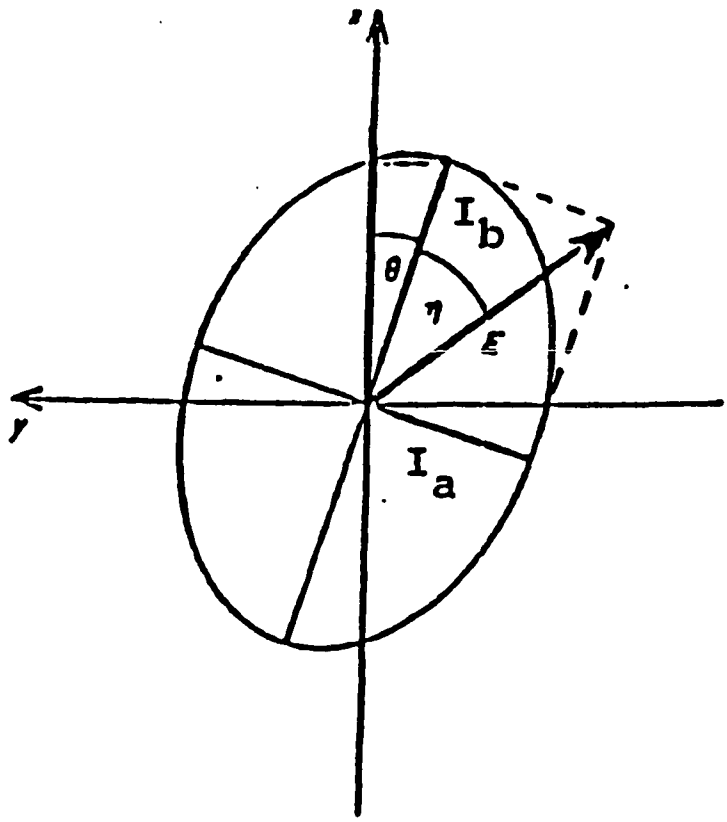

Figure 13. Polarization ellipse.

by

$$\eta = \text{arc tan } (I_a / I_b)^{1/2}$$

$\Delta\alpha$, $\Delta\varepsilon$ specify the finite cone of collection optics (Fig. 14). It is obvious from the above equations that large artefacts can arise from ellipticities deviating from 45°. If the azimuth is different from 45°, artefacts will be seen. Keeping the cone of collection angle small will help reduce the artefacts, too. However it should not be made too small in which case unacceptable intensity losses will occur.

The two equations are identical except for a factor of $-1/3$ and the dependence on $\sin^3\Delta\varepsilon/2$ in the depolarized component. It is clear based on these differences, that the polarized component is more succeptible to artefacts than the depolarized one. The $(1/\rho)$ dependence explains why polarized vibrations are more prone to artefacts than the depolarized ones. The term $\cos 2\eta \cos 2\theta$ can be taken as a measure of the artefacts, and EOM alignments are pursued in our efforts of minimizing this term.

The artefacts described by equations IV.4 and IV.5 appear as mono-signate signals. There is a further artefact which has drawn attention in the recent years. This artefact arises due to beam deflections during the modulation process (46) and appear as first derivatives. These can easily be misinterpreted as true ROA couplets.

The origin of the beam deflection will be considered next. The beam deflection artefacts were discovered when

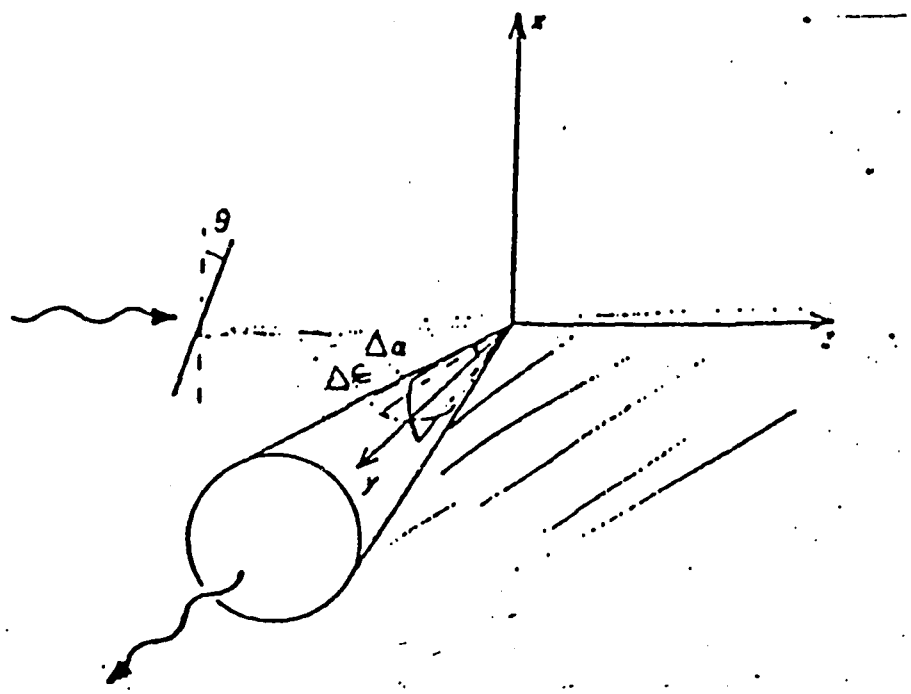

Figure 14. Scattering geometry (from Reference 20).

with a supposedly well aligned EOM ($\theta = \eta = 45^{o}$), occasional bad data with derivative-shaped artefacts were encountered.

It is extremely critical that the laser beam direction is exactly parallel to the crystal z axis (vide supra). In a slightly misaligned EOM, this is not the case. When a potential is applied along the z direction, the changes in the refractive indices along the x and y directions may cause beam deflection through the crystal as shown in Fig. 15. This beam deflection will depend upon the degree of misalignment of the EOM. It was realized that the new artefacts described in the last paragraph were due to these deflections of the beam during the modulation process. Due to the beam movement, the image at the detector is moving, and consequently the scattered light is detected via different diodes resulting in shifted peak maxima. Hence, difference spectra will appear with first derivative shaped artefacts.

These beam deflections are difficult to quantify. We find that a small pinhole, placed in the laser beam can be used to monitor deflections, since a deflection then will cause a change in intensity of about 1 to 2 %. The intensity changes caused by the beam's motion with respect to the pinhole can be related to the actual dispacement via the following procedure.

The total intensity of a laser beam profile (1.3 mm at $1/e^2$ point) in the TEM_{oo} mode is calculated first by nume-

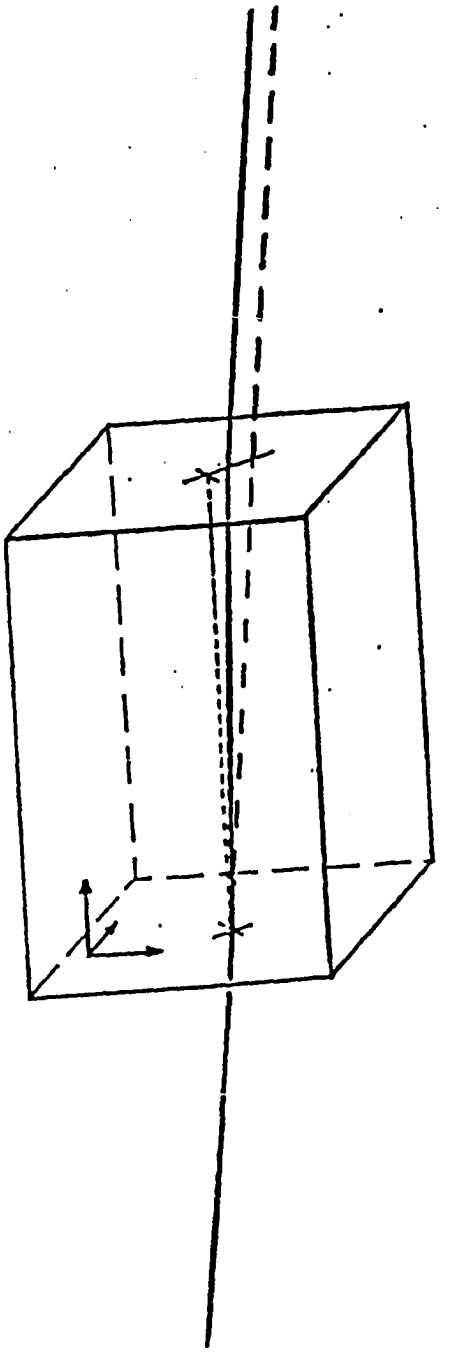

Figure 15. EOM and beam deviation

rical integrating a Gaussian profile (Fig. 16, top). Quantitative determination of the beam deflection may be obtained by a similar integration of the beam profile emerging from a 1 mm pinhole placed concentrically about the beam (Fig. 16, middle). If the beam is deflected, a situation depicted in bottom of Fig. 16 arises. The numerical integration calculations are carried out for several theoretical dispacements. A correlation of the displacements and the percentage change in intensities can then be made. Table I reflects the results of these calculations. It is observed that typical variations in the intensities amount to as much as 50 μm of beam deflections.

3. EOM alignment and reduction of artefacts

A perfectly aligned EOM guarantees an artefact-free spectrum, but is hard to achieve. In essence, alignment of the EOM amounts to measuring the Stoke's parameters (27) of the beam emerging from it and making appropriate adjustments until proper values for the various parameters η, θ and I (vide supra) are obtained.

The beam optics employed in the EOM alignment procedure has been described before (Fig. 9). In the Hunter College ROA instrument the beam parameters are extracted using a single set of measurement. As seen in the flow diagram (Fig. 17), the ellipticity, the azimuth, the intensity and the $\cos 2\eta \cos 2\theta$ term are all determined in one step. The EOM alignment program is capable of plotting out the $I(\Phi)$

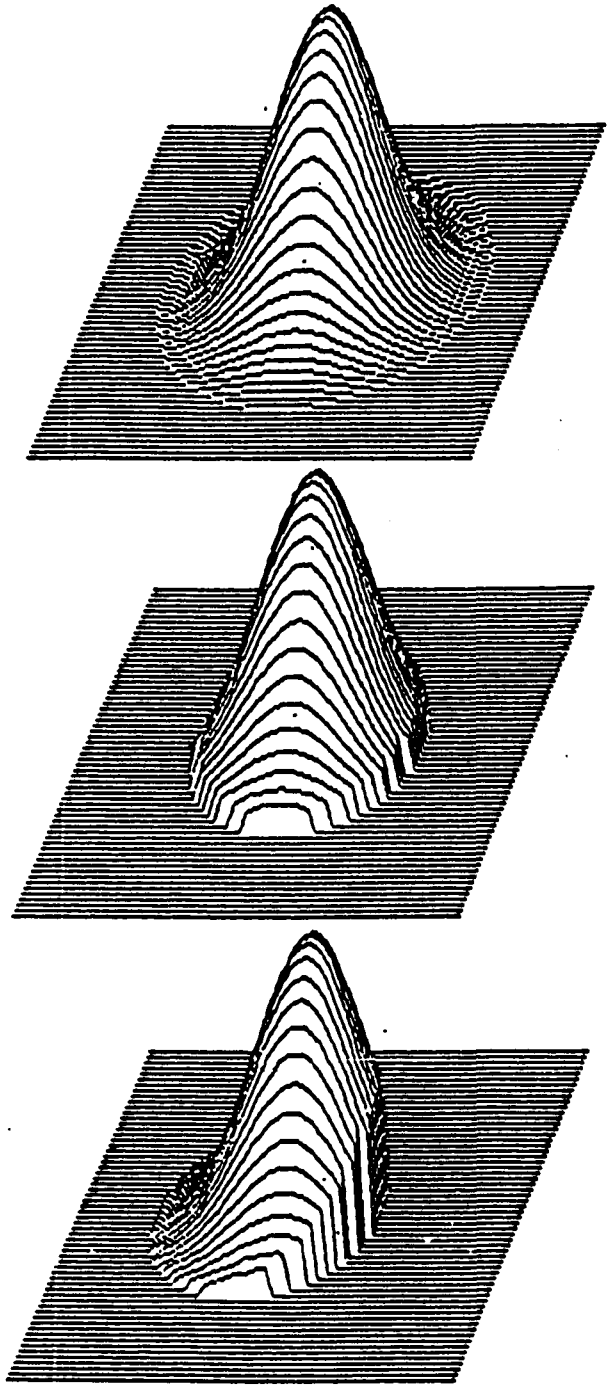

Figure 16. Laser beam profiles

TABLE I

Integrated Beam Intensity Profiles as a Function of Displacement[a]

Deflection[b]	Intensity[c]	% Change[d]	Comments
0	3.141	--	no pinhole
0	2.195	--	1 mm pinhole
1	2.183	0.5	
2	2.148	2.1	
3	2.091	4.7	
5	1.917	12	

a) Assumed Parameters:
Beam diameter : 1.3 mm at $1/e^2$ point
Pinhole Diameter : 1.0 mm

b) Beam Deflection : in units of 1/30 beam diameter (ca. 40 μ)

c) Arbitrary Units (Total Integral over TEM_{00} Profile = 3.141)

d) Intensity Change with Respect to 1 mm Pinhole, no Deflection

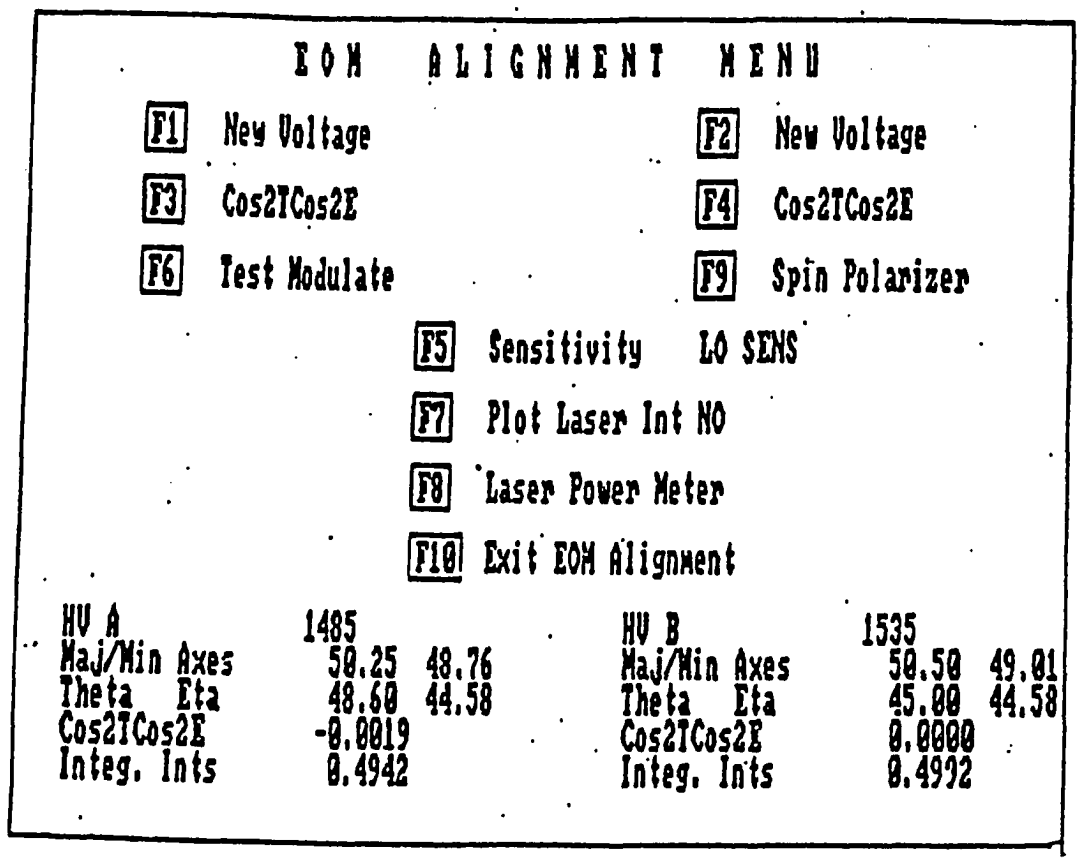

Figure 17.

vs Φ plot (see below), which serves as an elegant way to follow the alignment procedure (Fig. 18).

The procedure for the EOM alignment is as follows: With the focusing lens, the beam expander and the sample cell swung out of the optical path, the beam is aligned via two precision pinholes (1mm diameter) mounted along the vertical optical rail -one placed after the 45^{o} mirror and another after the sample chuck. The parallelity of the laser beam to the optical rail is confirmed when the laser beam passes through the two pinholes simultaneously. The pinholes are swung out of the beam and the beam expander inserted . After the alignment of the expander, the beam is allowed to pass through the EOM and the rotating polarizer. Subsequently, the beam strikes the laser power meter head (vide supra), the current output of which is passed into current-to-frequency converter, and a signal proportional to the intensity at the detector is read directly by the computer.

The next step in the alignment of the EOM is to center the beam in the EOM crystal maximizing the light throughput. The EOM is then rotated out of the beam, the polarisers are crossed and minimum intensity reading (usually less than 0.2% of the maximum reading) is read. With the EOM in the beam, this reading must be reproduced with less than 1% error. This procedure is to ensure that the EOM, without applied voltage, does not produce a rotation of the polarization ellipse.

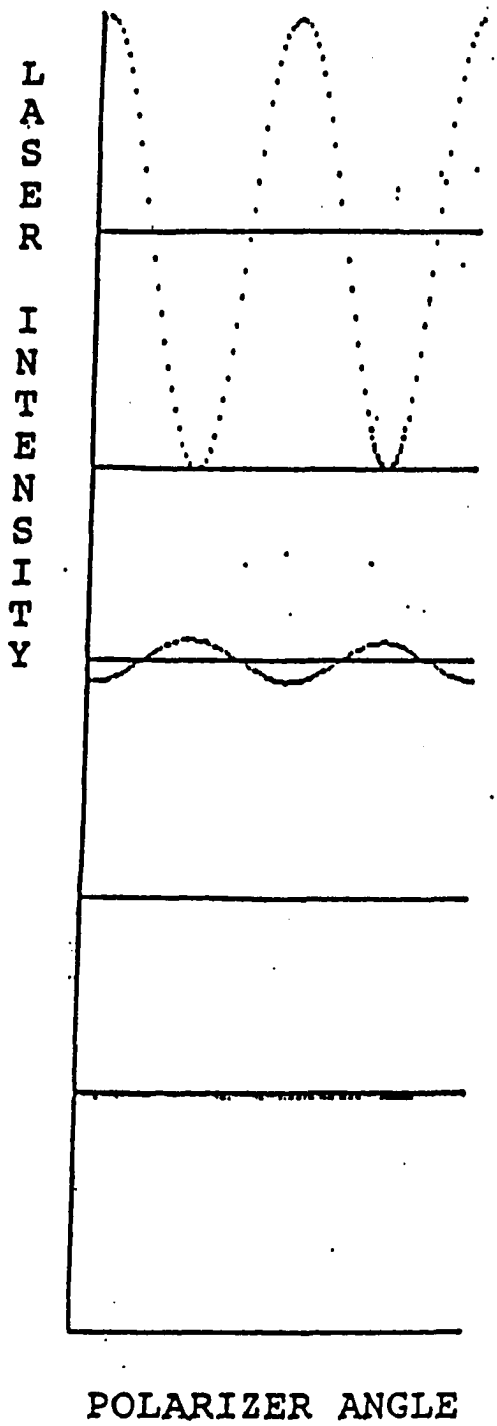

Figure 18.Plots of $I(\Phi)$ vs Φ

Next, the position of the rotating polarizer, at which the maximum intensity is observed with no voltages applied (the zero position, cf. Fig. 18), is determined. For linearly polarized radiation, the intensity at the detector as a function of the angle Φ between the laser polarization plane and the polarizer is, of course, given by

$$I(\Phi) = I_0 \cos^2\Phi \qquad \text{IV.6}$$

where I_0 is the intensity at the power meter for $\Phi = 0$. The polarizer is then rotated by 360° about the laser beam in 200 steps and intensities transmitted at each step are read and stored in an array. The maximum (I_a) and minimum (I_b) intensities are determined and η is calculated using the relation

$$\eta = \text{arc } (\tan I_a/I_b)^{1/2} \qquad \text{IV.7}$$

The azimuth of the polarization ellipse can be determined from the position of I_a (the maximum intensity) in the array of intensities. This is, because they are spaced by 1.8°. Ideally, for an unrotated ellipse, I_a should be the first element in the array (cf. Fig. 18). Clearly, the resolution available to localize I_a is 1.8°, which is just about sufficient for the alignment of the EOM. This actual measurement is performed by a procedure named Rotpol (Fig. 19). The polarizer is then returned into the zero position of maximum intensity. The entire procedure takes about 8 s.

Next the total intensity of the beam is determined by integrating over all $I(\Phi)$ values.

$$\int I_0 \cos^2\Phi \, d\Phi = \pi I_0 \qquad \text{IV.8}$$

Flow Diagram of the Polarization/Deflection Measurment Program

Main Program:

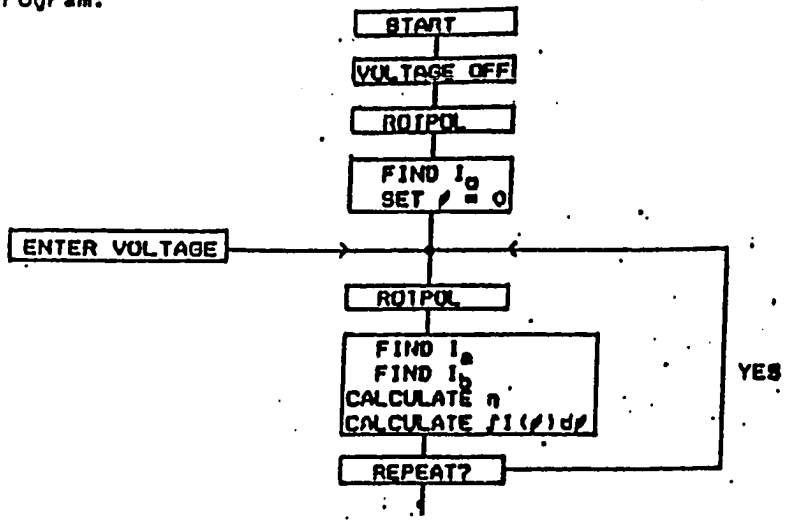

Subroutine ROTPOL:

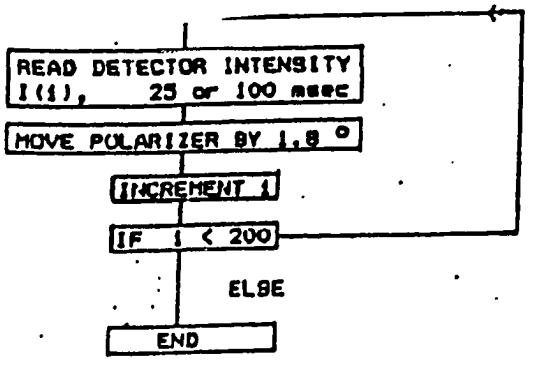

Figure 19.

where Φ is the polarizer angle (area as in 20b, c, or d). The total integrated intensity at the detector should be close to 0.5 (in units of $2\pi I_o$), irrespective of the polarization of the light produced (Fig. 20a vs 20b, c or d). This fact is important since it allows us to monitor the beam intensities and detect beam deflections. In cases where there is beam deflection, the total integrated intensities (TII) will be reduced from the theoretical limit of 0.5.

With a voltage applied to the EOM, the rotating of the polarizer is repeated and the beam parameters are derived. The decrease in I_b and increase in I_a observed indicate introduction of ellipticity of light and the shift in the position of I relative to its initial position will be a measure of θ , the azimuth.

A perfectly aligned EOM should give a plot as shown in the bottom of the Fig. 18 which is almost a straight line with maximum or minimum positions colinear with initial polarizer position (top trace in Fig. 18)

The EOM alignment procedure is a systematic, step by step process. With low voltages, usually about 1000, the pitch and yaw and rotation of EOM are adjusted till the η values for both polarizations are close and θ values are both equal to 45°. Intensities are monitored simultaneously. The voltages are gradually increased in steps of 50 to 100 volts, until ellipticities close to 44° are obtained. η, θ and I values are monitored carefully at each

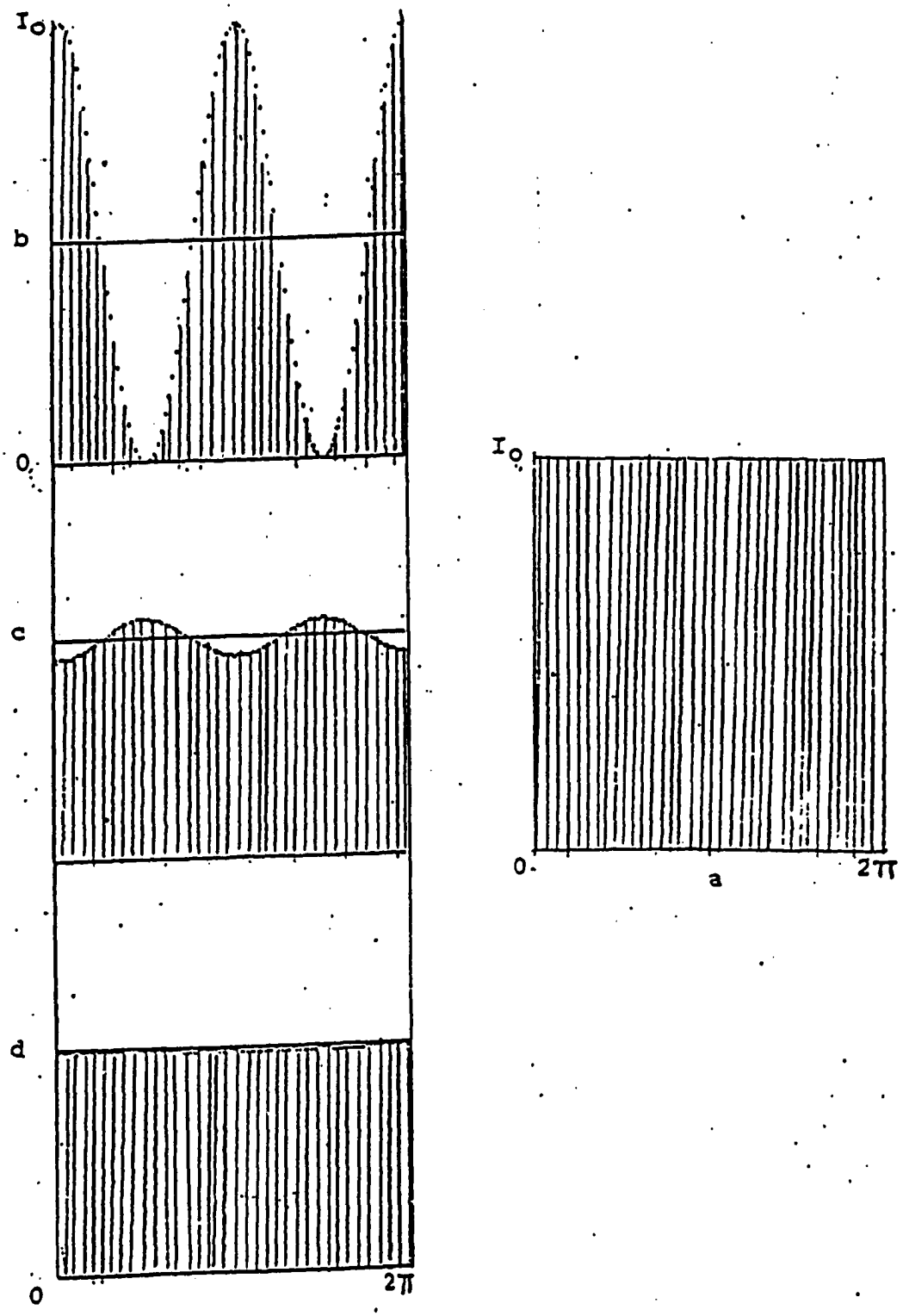

Figure 20. Areas under intensity plots

step. Identical values of $\cos 2\eta \cos 2\theta$ for both polarizations as well as total integrated intensities of 0.5 are aimed for. Owing to the residual birefringence of the EOM, this might not occur at equal voltages for the two polarization states. For the EOM used at Hunter College, it is observed that a difference in voltages about 60 volts for 514.5nm gives the best alignment with the least beam deviation artefacts. A difference in the I values of <0.1 % is tolerable.

When the alignment is nearly perfect, fine adjustments are made switching to high sensitivity mode (F5 in Fig. 17). In this high sensity mode, the procedure of rotating the polarizer is carried out at a slower pace. At each position of the rotating polarizer, the power meter is read at least three times longer. This procedure reduces the read out noise in the measurement of the beam parameters.

If one of the applied voltages is greater than the $\lambda/4$ retardation voltage, over-modulation results. This will flip the ellipse (Fig. 18; middle plot) and will lead to $\cos 2\eta \cos 2\theta$ artefacts of opposite signs which will get doubled in the dual lens system (vide supra). Hence, over-modulation is undesirable and carefully avoided. Voltages are reduced by 2-5 volts after the final alignment. Though this might result in increase in ellipticities, these artefacts cancel in the dual lens set-up (vide infra).

Finally it is possible to reduce a certain level of spurious signals by means of data treatment. In our instru-

ment, the intensity data due to left and right circularly polarized light are coadded and stored separately (although the real time display shows the actual sum and difference spectra). Storing the data separately offers the possibility of of scaling one data set with respect to the other to compensate, for example, for a long term laser intensity drift which is not cancelled via the modulation. In some of our data sets, such scaling (by about 0.1 %) has improved the symmetry, about the baseline, of enantiomeric spectra. Likewise, shifting the data sets with respect to each other, by an amount corresponding to about 0.01 diode, will reduce the spurious results due to beam deflections. However this method of data treatment to reduce our artefacts, is seldom preferred to the proper and more elegant method of aligning our EOM to its very best.

D. Collection optics alignment

After the alignment of the EOM, the light collection system has to be adjusted so as to equalize the intensities through the two collection arms. The dual system will defeat its purpose, if the scattered intensities through the two arms are not equal. According to (20), for the collection optics with its axis at +45 to the y axis, the incident azimuth is effectively θ -45 whereas for the other arm it is θ +45. Thus, the equations for the artefacts collected through the two arms are:

$$[\cos 2(\theta_R - 45^\circ) - \cos 2(\theta_L - 45^\circ) + \cos 2(\theta_R + 45^\circ) - \cos 2(\theta_L + 45^\circ)] = 0 \qquad \text{IV.9}$$

It is obvious from the above equation that the two arms experience artefacts of opposite sign that cancel upon addition.

The procedure of balancing the intensities through the two arms involves the collection of Raman spectra through one arm at a time using computer controlled shutters. The intensities so collected are subtracted from one another and the difference is displayed in real time. This difference spectra will give clues as to the sources of the difference, and accordingly, the optics are adjusted. For example, derivative shaped differences are due to the fact that the recombined images do not coincide and can be reduced by adjusting the position of the recombination optics.

Balancing the intensities for both arms will help cancel the artefacts due to ellipticities and rotation of the ellipse as mentioned above. However, the residual intensity deflections will cancel each other only when the direction of the beam deviation, if any, is kept along the plane of the incident beam in a dual lens ROA spectrometer. However, it may prove worthwhile to reduce the image magnification of the light collection since this will reduce the deflection of the image at the entrance slit of the monochromator.

The collection optics alignment procedure is considered satisfactory when a difference spectrum, expanded at least

ten times, shows no bias or derivative shaped signals.

E: Collection of ROA data

The actual measurement of ROA data, which follows the different alignment procedures, is discussed in this section.

Once the EOM is aligned for minimum ellipticities and beam deflection and optimum azimuth, and once the collection optics are aligned for equal scattered intensities for the two arms, a ROA data acquisition can be initialized. The modulation sequence is as follows: High voltage A is switched on which reaches quarter-wave retardation potential in 25 ms. Data accumulation is started after three 'clear' cycles to erase the detector. Data are integrated on the diode array for a preselected integration time (see below). The diode array may be read a pre-set number of times during a modulation half-cycle and the data obtained in this modulation half-cycle are stored in one data array. Subsequently the other voltage B is turned on and the voltage A turned off creating opposite circular polarization. As before, after a delay and several diode clear cycles, the intensities are read and stored in another separate array. Both the sum (A+B) and the difference (A-B) spectra are displayed and the improvement in signal-to-noise ratio in both traces can be followed in real time.

Depending on the light levels of the detector, different sequences for ROA data acquisition may be specified.

For low light levels, long integration periods (about 10s) are required. In such cases, the high voltage sources are switched every modulation half-cycle. This is advantageous since the diode array should be read as few times as possible to reduce readout noise; however saturation of any diodes must be avoided. For high light levels (neat liquids like pinène), the diodes will be saturated within very short times (.5- 1 s) which would require higher modulation frequencies. This presents difficulties because the EOM requires at least 200 ms to stabilize, although the voltages reach their plateau much faster. Thus, in cases where high light levels are encountered, the diode array is read between 4 and 16 times, during each modulation half-cycle. The intermediate scans are coadded within the diode array controller board (for details, see Ref.21).

Data sets with total intensity values greater than 10^7 are stored on disc and then used for further data manipulation like smoothing, coadding, and linearization. Linearization is a process, described in detail in (47) to convert the diode array data collected into linear wavelength or wavenumber.

F. Determination of the sense of circularity of light produced

In ROA, the experimentally determined quantity is given by

$$\Delta = (I_R - I_L)/ (I_R + I_L)$$

It is necessary to know the sense of circularity of light produced by the application of a certain voltage in order to ascertain if the difference obtained is (I_L- I_R) or (I_R- I_L) and calibrate the results accordingly.

It is possible to determine the sense of circularity of light produced by the EOM by optically combining it with a reference source of circularly polarized light of known handedness.

In the Hunter college lab, a simple experiment is carried out to facilitate the above measurement.

The definition of right or left circularly polarized light as it is adopted by Jenkins and White(3) and accepted by Born and Wolf as the "traditional" nomenclature of circularly polarized light (48) is employed. Light is said to be right circularly polarized when to an observer,facing the source, the electric vector seems to rotate in a clock-wise fashion with respect to the time axis.

A quarter-wave plate is used with the EOM to determine the handedness of the light produced by the EOM. An uni-axial crystal which exhibits birefringence can be cut into a plate of right thickness so that the two vibrations of the light emerge out 90^0 phase-shifted. The relation uti-lized is as follows:

$$\delta = 2\pi/\lambda\, d\, (n_O - n_E)$$

where δ is the phase-shift, d the thickness of the crystal, n_O and n_E denote the refractive indices of the ordinary and extra-ordinary rays respectively. λ is the wavelength of

light employed. 90^0 shift will correspond to a path difference of $\lambda/4$, and the plate is then called a quarter-wave plate. If plane polarized light enters the quarter-wave plate placed such that the slow or the ordinary axis (as indicated by a line on the mounting) is 45^0 to the plane of polarization from the point of observation, then the circularly polarized light produced is right-handed.

The conclusion about the sense of circularity is based on the following argument:

If the quarter-wave plate is positioned to produce right circularly polarized light, and if the EOM also produces right circularly polarized light, then the two quarter-wave retardations should add up (equivalent to half-wave retardation) and the resulting light should be plane polarized light but the plane of polarization ellipse will be rotated through 90^0 with respect to the original plane of polarization. On the other hand, if the EOM produces left circularly polarized light, the quarter-wave retardations of opposite signs should cancel out each other resulting again in plane polarized light. However, now the plane of the polarization ellipse is not rotated but retains the original angle.

The beam parameters are read in the usual manner (see alignment of the EOM section) using the rotating polarizer for different relevant settings and the readings recorded (Table II). Cases (iv) and (v) demonstrate that voltage A produces left while B, right circularly polarized light.

Table II . Experiment to determine the sense of circularly polarised light produced by the EOM using a quarter-wave plate.

case	conditions	EOM voltages	η	θ
(i)	NO quarter-wave plate	A = 0 B = 0	2.11	45
(ii)	quarter-wave plate IN	A = 0 B = 0	20.2	135
(iii)	quarter-wave plate IN	A = 600 B = 0	28.8	38.5
(iv)	quarter-wave plate IN	A = 0 B = 650	2.19	135
(v)	quarter-wave plate IN	A = 1900 B = 0	2.20	45
(vi)	quarter-wave plate IN	A = 0 B = 1900	30.6	38.3

Cases (iii) and (vi) ascertain the invalidity of the other alternative. In the data accumulation scheme, ROA signals are calculated by subtracting intensity in channel B from that in A; hence, the ROA data corresponds to($I_L - I_R$)

It is observed from Table II, that in this experiment the voltages used for the EOM are below (cases iii and iv) and above (cases v and vi) the typical retardation voltages employed to run ROA experiment. The reason for this is as follows: The quarter-wave plate used is likely to be designed to act as one for 632.8 nm (He-Ne line). Thus for 514.5 nm, it is more like a $3\lambda/8$ plate (case ii).

In order to produce $\lambda/2$ retardation, one needs only $\lambda/8$ retardation in the same direction which explains case iv. In a similar fashion, to cancel the retardation produced by the quarter-wave plate, the EOM should produce $3\lambda/8$ retardation in the opposite direction. This is the reason for using in case v, a voltage excess of the quarter wave potential.

V. RESULTS AND DISCUSSION

A. Introduction

The small magnitude of the commonly observed ROA signals (of the order of 10^{-4}) makes it difficult to collect new ROA data of significant S/N ratio. Very often, data has to be collected for several overnight scans and coadded together. In a system where minute variations in conditions like temperature create major undesirable changes (for example, the EOM alignment parameters), long accumlations do not offer many advantages.

In this chapter, ROA data of α-pinene will be discussed first. This is then followed by an attempt to correlate quantitatively the beam deflection artefacts with the EOM alignment parameters (vide supra). ROA data of chlorofluoro acetic acid and cyclic AMP will be discussed in the last section.

B. Discussion of ROA data of α-pinene 

Pinene has been accepted as the universal standard to evaluate the performance level of a ROA instrument. There are two main reasons for this; first, pinene is commercially available in optically pure forms; second, the pinene couplet at 780 cm^{-1}, which is due to CH_2 rocking vibrations, is large enough (of the order of 10^{-3}) to be observed easily. In Fig 21 is shown the depolarized data of α-pinene acquired at Hunter College. The data acquisition time for this spectrum was about 10 h at a laser power of

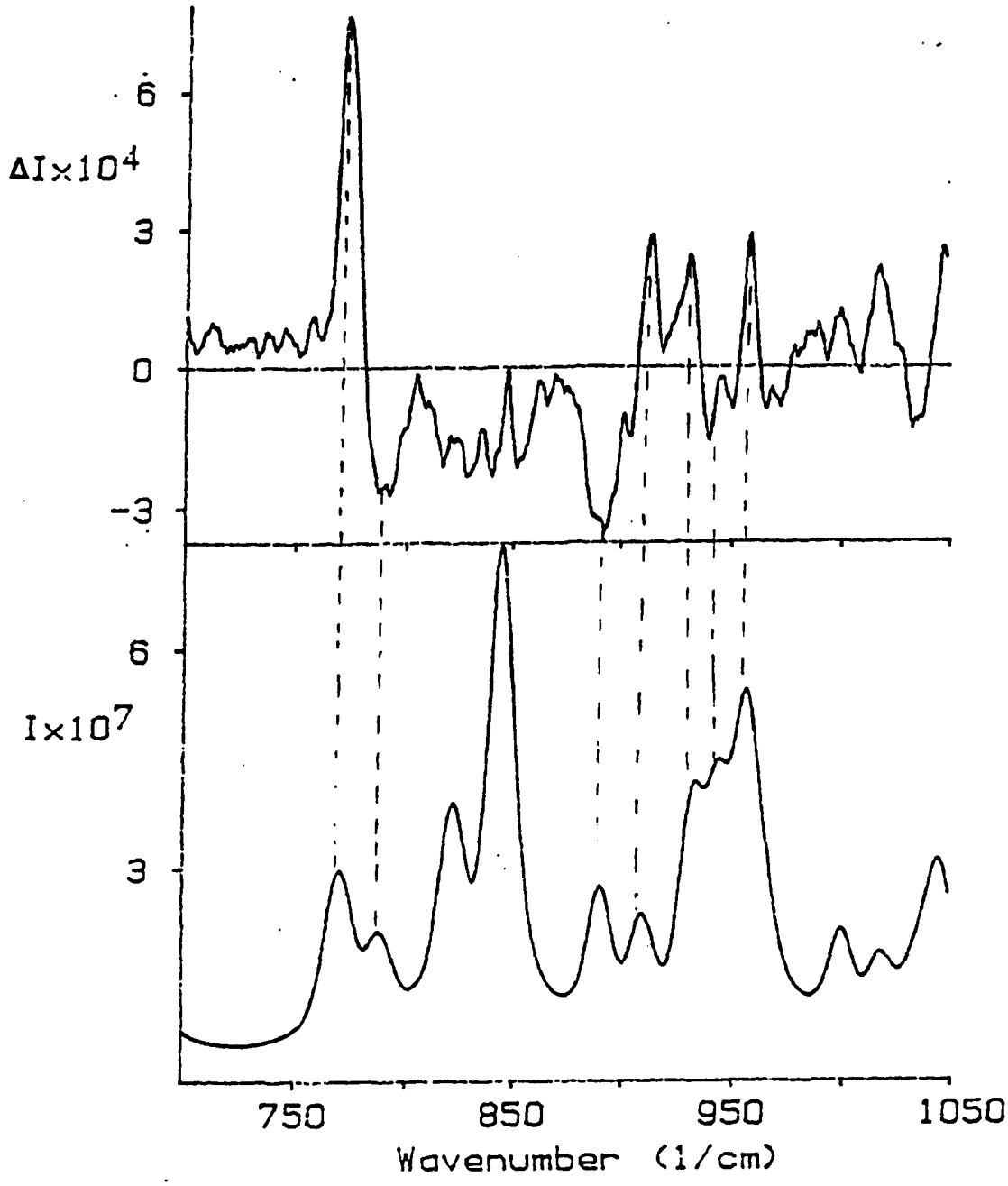

Figure 21. Depolarized ROA of α- pinene

500 mW at 514.5 nm and the slit width was about 150 μ. The spectrum is devoid of any artefacts and exhibits a good signal to noise ratio. All ROA signals marked with the vertical dashed lines compare remarkably with the literature results and are well-defined.

The depolarized component is observed commonly since it has been proved to be affected the least by artefacts (vide supra). However the polarizer drastically reduces the light throughput and the collection of data with accetable S/N ratio takes a long time. In the Hunter College lab, data were collected without using an analyser to overcome this problem (total ROA). In Fig. 22, is shown the total ROA data of ± pinene. The data acquisition time for this spectrum was about 3 hr at a laser power of 500 mW at 514.5 nm. Considering the fact that the total ROA has the the most artefact-succeptible polarized components, the spectra presented here demonstrate the level of EOM and table top alignments achieved in our lab. In Fig.23, is shown the ROA data of the two enantiomers of α-pinene. The acquisition times were about 2 h for each enantiomer The mirror image features of the different ROA signals of the two enantiomers is indeed striking.

C. ROA data of (+) 3-methylcyclohexanone 

In Fig.24 is given the depolarized data of (+) 3 methyl cyclo hexanone. This molecule being a neat liquid is another one suited for study. Also, a lot of electronic CD

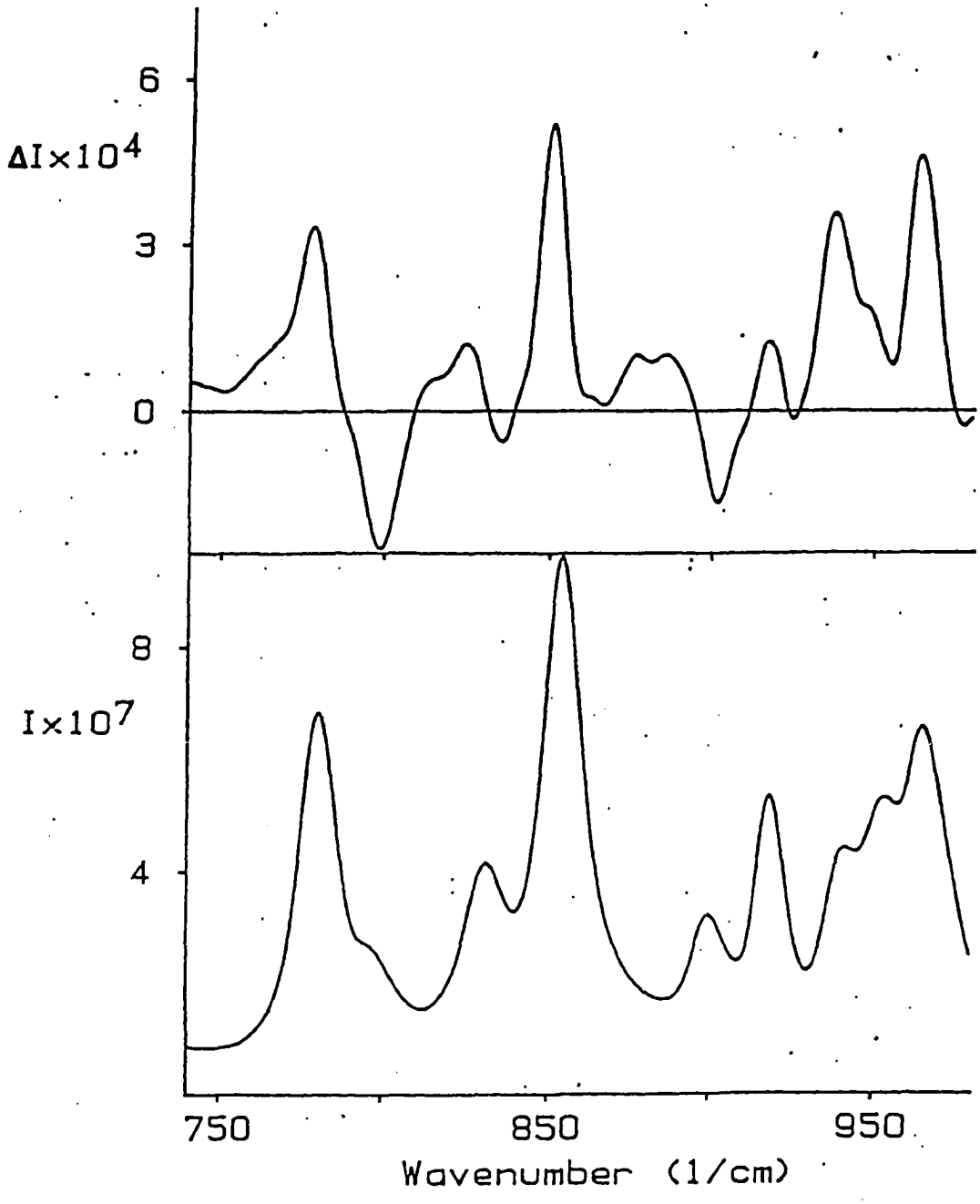

Figure 22. Total ROA of pinene with EOM alignment II

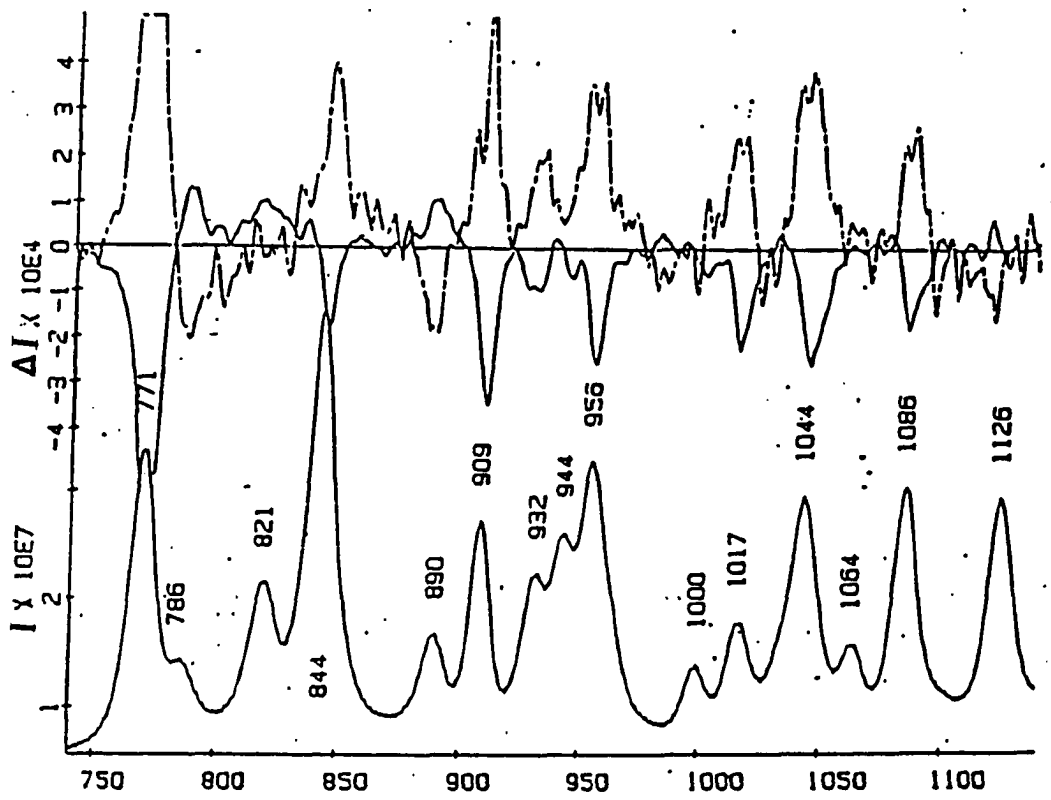

Figure 23. Total ROA of (±)α-pinene.

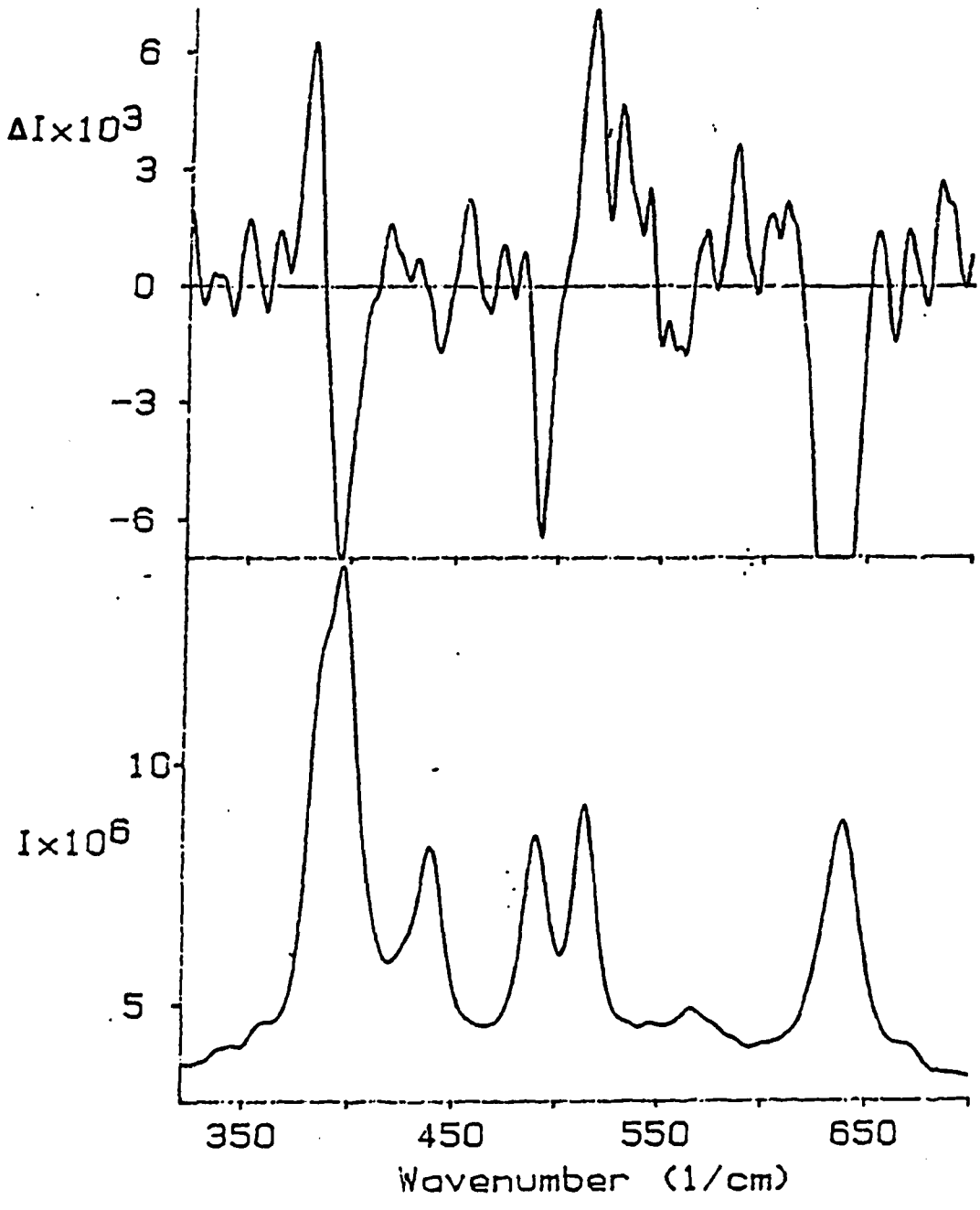

Figure 24. Depolarized ROA of (+) 3-methylcyclohexanone

has been done on this molecule and it has been used as a model for the interpretation of electronic CD signals. Nafie and coworkers have carried out normal co-ordinate calculations and isotope studies on this molecule (49). The low frequency region was assigned to 11 skeletal modes. The origin of the couplets in this region was explained as arising from the chiral perturbation by the methyl group, which mixes the achiral skeletal modes of the cycloheaxanone ring. Nafie and his group did molecular orbital calculations using the atomic polar tensor model for ROA (49). The experimental results agreed well with the calculations for the skeletal vibrations. The ROA data collected for (+) 3- methyl cyclo hexanone in our lab (Fig.24) is identical with the published results of Nafie (49).

D. Quantitative study of the derivative-shaped artefacts

The artefacts due to ellipticities and azimuths differing from 45°, have been investigated by others (20) and proved to be proportional to $\cos 2\eta \cos 2\theta$ (vide supra). Here, artefacts due to beam deflection, the origin of which has been discussed before, will be analysed. In this chapter, a quantitative correlation between the derivative shaped artefacts and the variations in the total integrated intensity parameters (TII) observed during modulation is sought.

It was shown before that, via a numerical method of integration of the Gaussian profiles, a percentage change in the TII parameters can be correlated with the beam

deflections. If a percentage change in TII of 0.1 % occurs during modulation, one can conclude that the beam deflection is about 8 μ (Table I). This beam deflection is magnified at least 5 times by the collection optics (vide supra), resulting in a deflection of about 40 μ at the entrance slit as well as in the detector plane. This beam deflection moves the scattered image over diodes of the array detector.

Though the ratio of the size of the image at the slit and the detector is in principle 1:1, the deflection of the beam by 40 μ cannot correspond to a motion of 1.6 diodes (diodes are spaced by 25 μ) for the following reasons: The laser beam profile is Gaussian in nature with a width of about 200 μ. However this profile will be distorted at the detector focal plane according to the slit transfer functions. The deflection caused will diffuse over the entire profile and produce a much less effect.

In our manipulation routines, an artificial shift can be created in the right direction to null the effect of beam deviation. In instances where the percentage change in TII parameters were about 0.1 %, it was observed that a shift equivalent to 0.05-0.08 diode had to be used.

From the above observations, it is concluded that a deviation corresponding to 0.1 % change in TII produces a rather small shift in the diode elements and this level of beam deviation artefact is not intolerable.

Keeping the above factors in mind, three different EOM

alignment procedures (vide supra) have been attempted in our lab.

In the first procedure adopted, an unexpanded beam is allowed to pass through the EOM and a precision pin hole placed in the beam path. ROA data of α-pinene collected using this alignment procedure is shown in Fig. 25.

In Fig.25 the ROA of pinene for each arm separately is presented. The acquisition times were too short to see any ROA and we were looking for artefacts only. The fact that only one arm showed large derivative shaped artefacts, indicates that the beam deflection was in a direction perpendicular to the optic axis of the collection lens through which the spurious signals were observed (vide supra). It is noticed that the derivative shaped artefacts were quite large. This has been forseen from the nature of a highly focussed beam. The unexpanded beam not only makes the beam deflections very significant, but can introduce more artefacts as follows: Local heating of the EOM crystal can change the refractive indices in the x and y direction, creating a birefringence. Also, more artefacts can be seen due to the inhomogenities of the EOM. Hence this procedure of aligning the EOM is highly unfavourable.

In a second method, an expanded beam is used. However, the EOM is aligned here without a pin hole in the beam. The ROA data acquired using such an alignment is shown in Fig.22. This data shows no derivative shaped artefacts. It is true that, in the absence of a pin hole, the beam

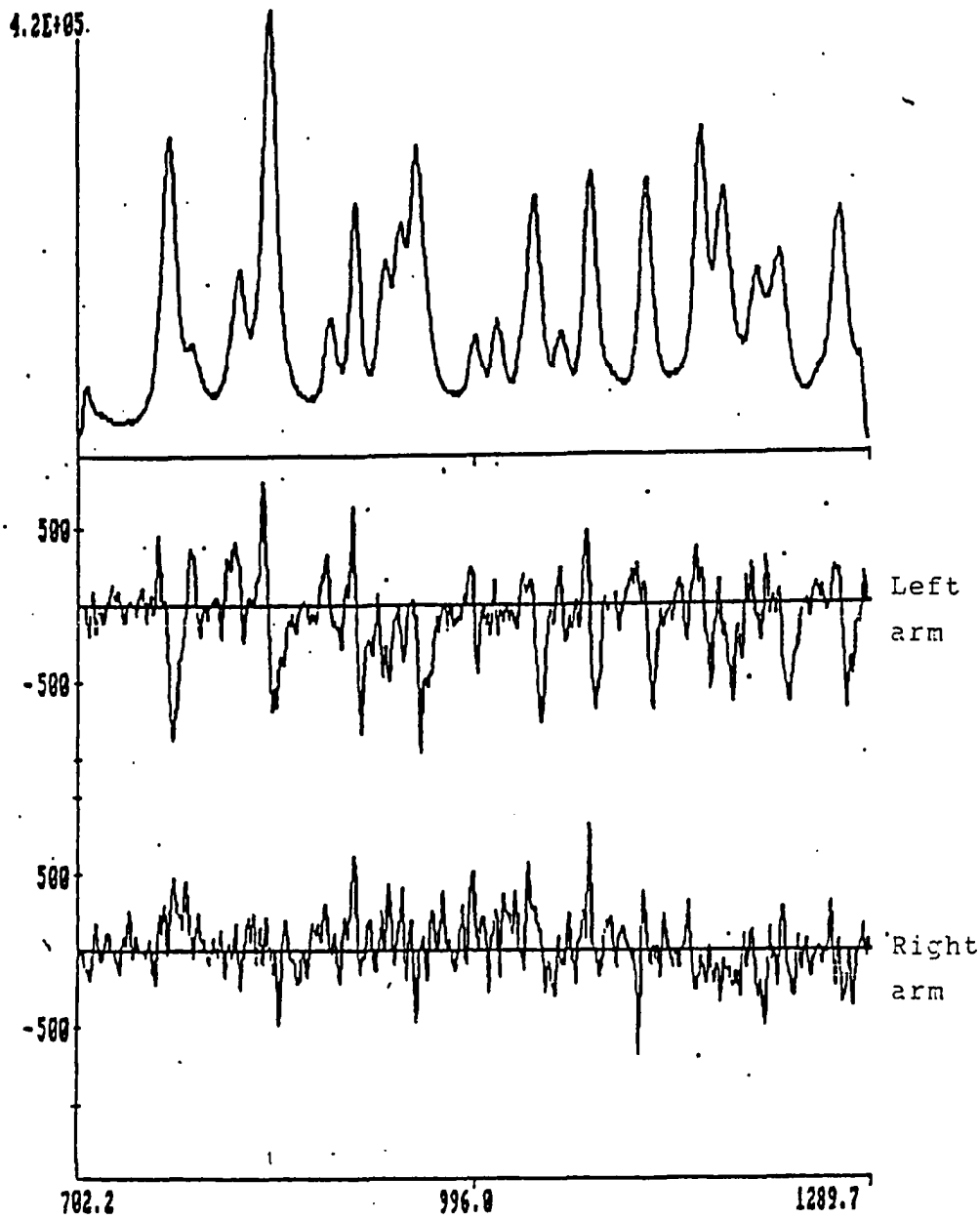

Figure 25. Total ROA of pinene with Eom alignment I

deflections could not be measured accurately. However, the detector has some pin hole effect and will detect deflections of reasonbly large magnitude. The absence of derivative shaped artefacts in this case indicates, therfore, that the deflections, if existed at all, were small.

The above procedure has all the advantages of using a expanded beam. In addition the EOM is the only optics which needs to be physically aligned. Hence this alignment procedure takes short periods of time and the alignment parameters have been found to remain stable for a period of at least one week.

In the third procedure, an expanded beam is used in combination with a pin hole. The sample focusing lens needs to be used to focus the beam into the pin hole. In order to converge the focused beam through the pin hole and into the laser power meter, a second focusing lens of very short focal length is introduced in the EOM alignment set-up (vide supra). The position of the pin hole is fixed where the intensity loss due to the pin hole is not more than 20 - 25 %. The position of the lenses were found to be quite critical and their alignments unnecessarily consumed major part of the time that could be used in the EOM alignment. The lenses have also been suspected to introduce birefringence and aberrations. In Fig.26 is given total pinene data collected via this alignment procedure.

A comparison of the two data (Fig. 26 and 22) does not favour in any way the alignment procedure with a pin hole.

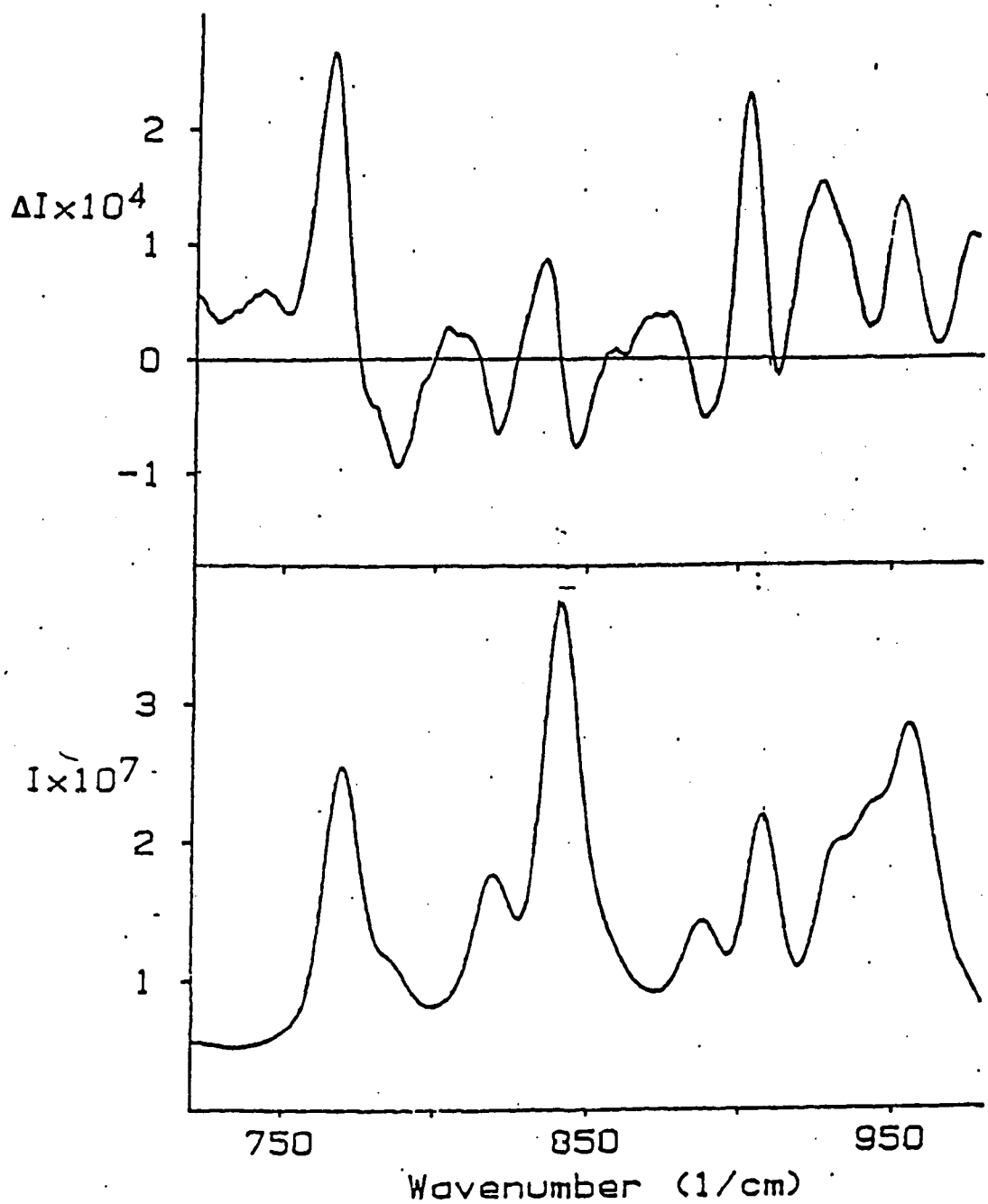

Figure 26. Total ROA of pinene with EOM alignment III

The conclusion derived from the above experiments is as follows:

Although a pin hole is necessary to detect beam deflections accurately, it would not be worthwhile to consider the third procedure (see above). It would be reasonable and practical to cancel small levels of beam deflections using the artificial shift factors in the manipulation routine. Lots of time could be gained and unnecessary misalignment problems created by the additional optics (focusing lenses in the third method) could be avoided. Thus the second procedure of aligning the EOM with an expanded beam with no pin hole or any other lenses in the beam path seems to be the best choice.

E. Discussion of ROA data of chlorofluoroacetic acid

Chlorofluoroacetic acid is one of the smallest non-cyclic chiral molecules. It is a neat liquid and the chiral synthesis is not very complicated. Thus this molecule is well suited for ROA studies. The normal co-ordinate analysis and vibrational assignment were reported by Calienni et al. (50).

In Fig. 27 and 28 are shown the ROA data of - (S)chlorofluoroacetic acid for three spectral regions. There are three small ROA signals observed at 357 cm^{-1}, 701 cm^{-1} and 1439 cm^{-1}. These frequencies correspond to Cl-C-F deformation, CO_2H wagging and C-O stretching repectively. A study of the nature of these vibrations led to the under-

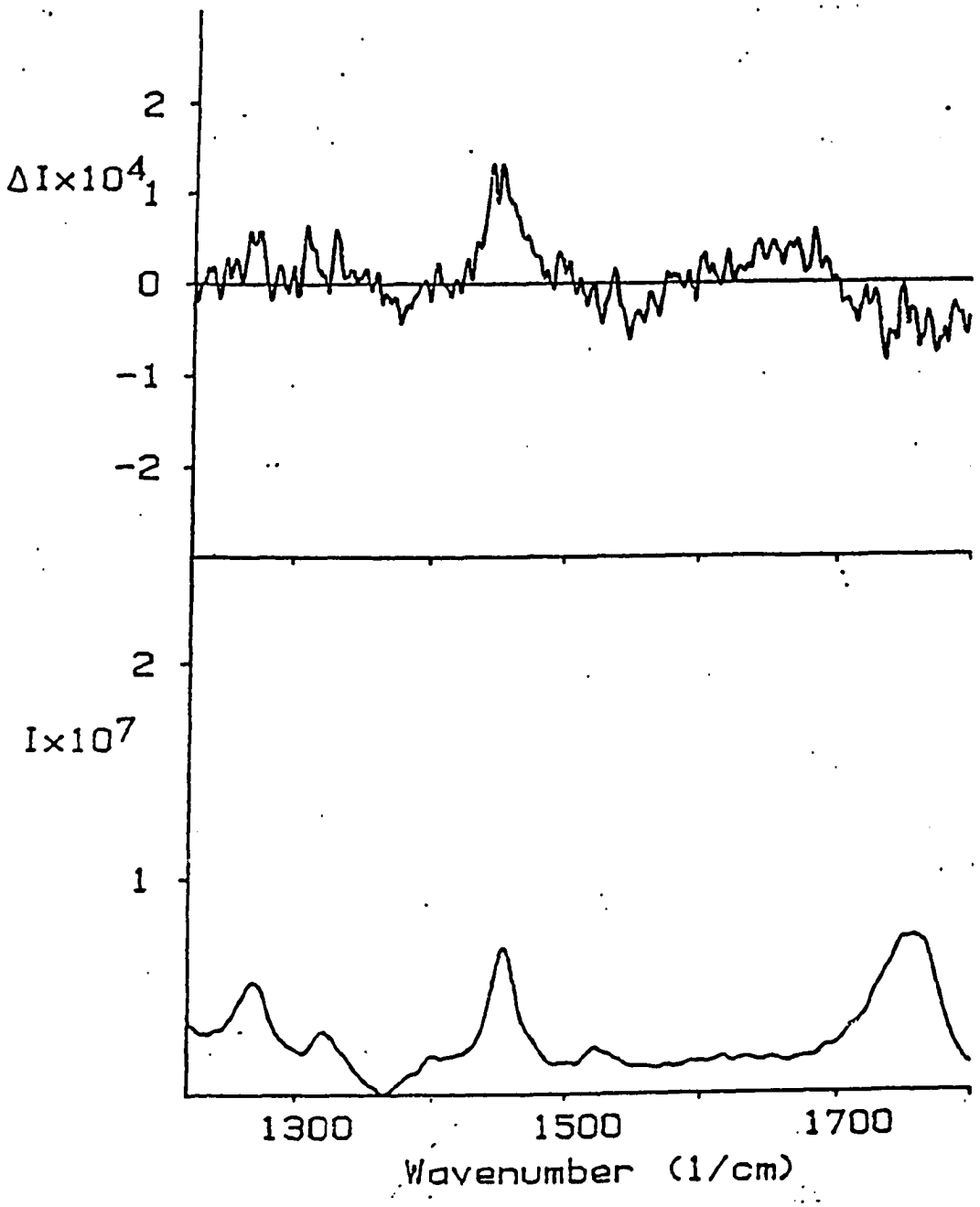

Figure 27. Total ROA of chlorofluoroacetic acid I

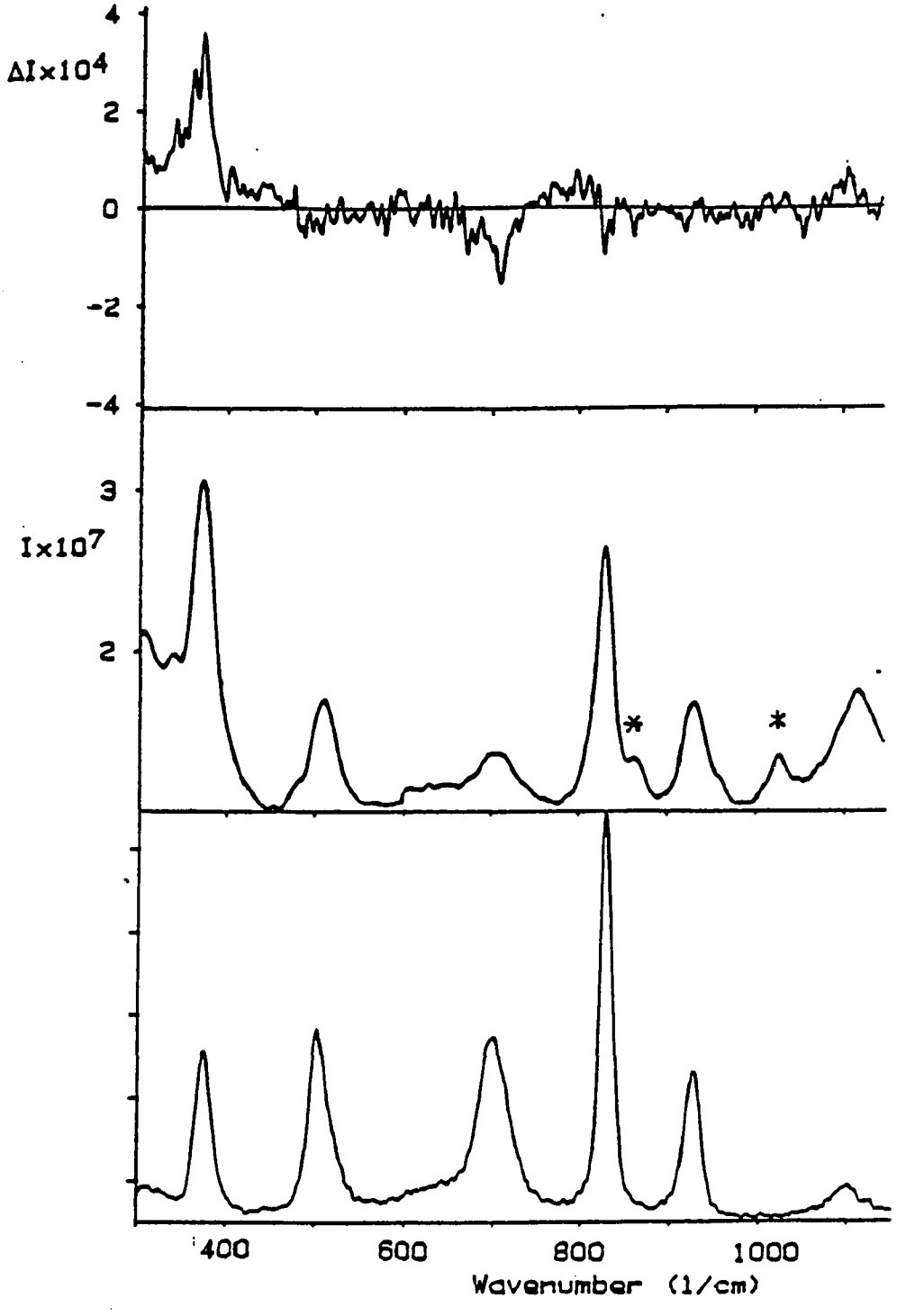

Figure 28. Total ROA of chlorofluoroacetic acid II

standing of the origin of the ROA signals at these frequencies (50).

All the vibrations in question involve large displacement of several atoms; in addition to this factor, it is observed that in each instance, there is a twisting of the molecule; the in-plane vibrations are strongly coupled with the out-of plane vibrations. There is a large distortion of the molecule; the motion in one part of the molecule affects that in a different part, and leads to the displacement of all the atoms in the molecule. The fact that the later condition is necessary to bring about ROA is supported by the follwing observation: The vibration due to C-C stretching occuring at 927 cm^{-1} shows no ROA. Though this vibration involves large motion of most atoms, nearly all the displacement vectors lie in the same plane and hence there is less distortion which leads to absence of any ROA signals (50).

F. Discussion of ROA of cyclic-AMP 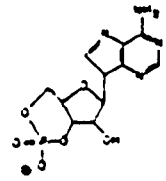

It is observed that in the absence of conformational freedom, no cancellation of ROA signals occurs. Large molecules and molecues which have rigid structures have less conformational freedom. α-Pinene is a typical molecule belonging to this category and as mentioned before is one of the few molecules with many large ROA signals.

Cyclic-AMP is another large molecule with a rather rigid structure. The normal Raman spectrum (polarized) is

shown in Fig.29. The aquisition time was about 10 h using a laser power of 500 mW at 514.5 nm. In Fig.30 are presented the depolarized Raman and ROA spectra. The spectral region shown here extends from 1050-1300 cm^{-1}. The high frequency region covered mainly the base skeleton and showed no ROA. The vibrationl assignments for the compound were obtained from Ref.51. An aqueous solution of cyclic-AMP at neutral p_H was used for the determination of ROA spectrum. Owing to the small magnitude of the signals, three over-night scans were collected and the data coadded later. ROA signals were found at the frequencies 1087, and 1252 cm^{-1} respectively. These correspond to symmetric POO^- stretching, and anti-symmetric POO^- stretching respectively.

As observed in the case of chlorofluoroacetic acid, the phosphate vibrations distort the different parts of the molecule to a large extent and produce ROA signals. The base vibrations are fairly localized and will not affect the motions of the atoms in other parts of the molecule.

In the cyclic-AMP data, all the positive features shown in Fig.30 were observed in every scan collected. The origin of these signals has not been clear and the interpretation unsuccessful. The cyclic-AMP data was collected in aqueous medium and this might account for the uncertainities observed and poor S/N ratio. We attribute the difficulties with solution of aqueous media to the large fluctuations in background.

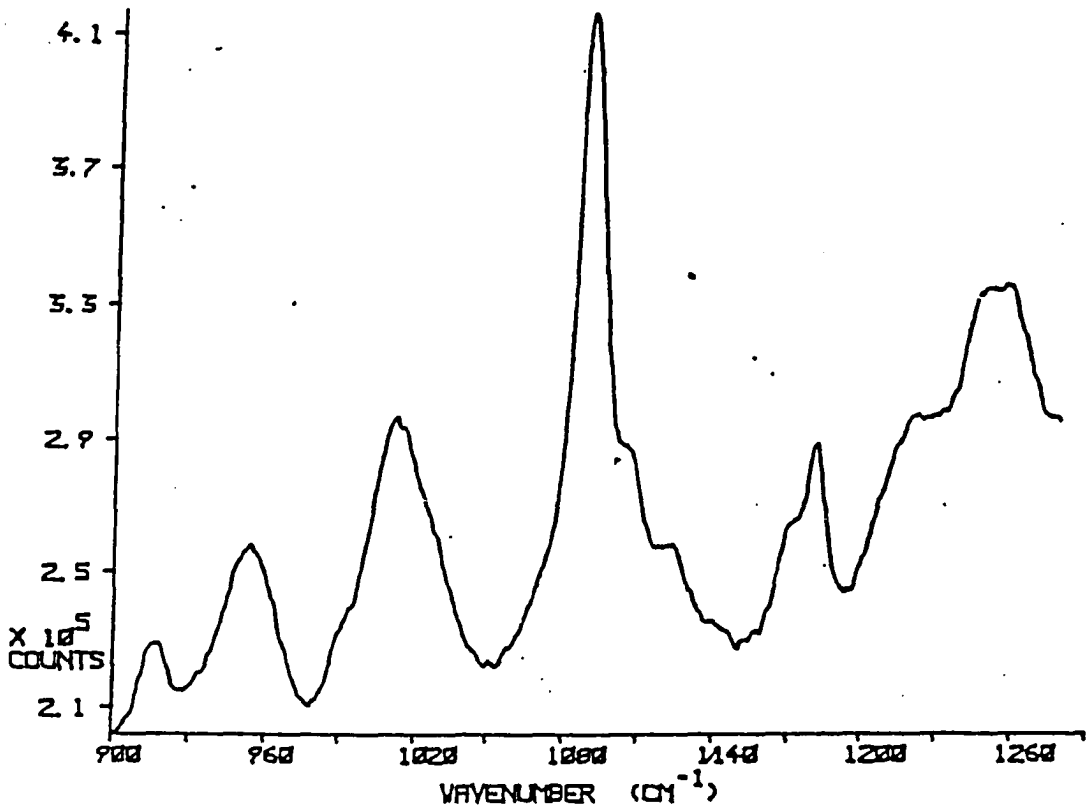

Figure 29. Raman spectrum of cyclic AMP

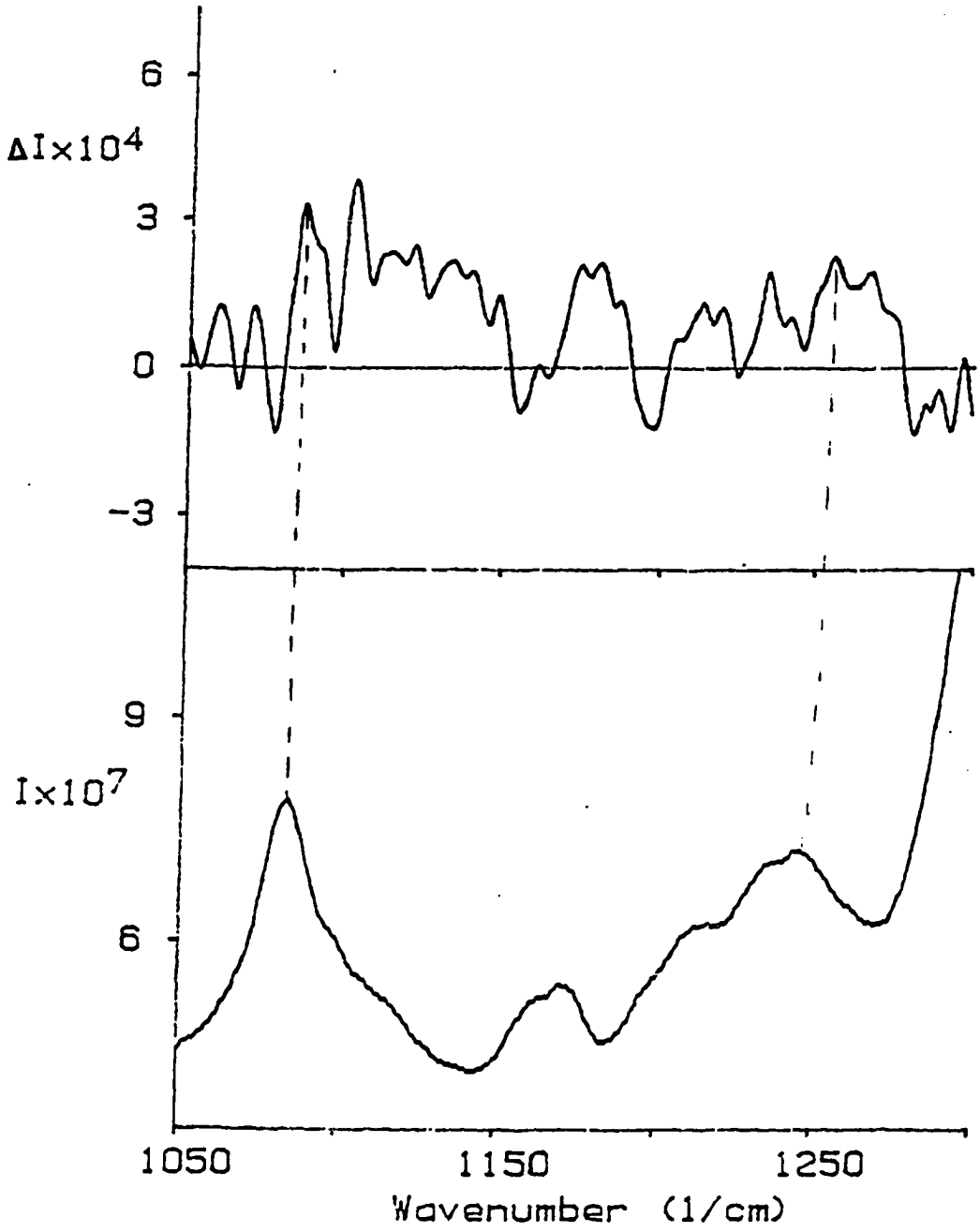

Figure 30. Total ROA of cyclic AMP

G. Conclusion

Aqueous systems pose serious difficulties because of the reduced scattered intensities and the increase in background noise. Also, in contrast to neat liquids such as pinene the molarity of the compound is reduced at least an order of magnitude while using a solution. The detection of such small signals is possible if the level of artefacts and noise levels in ROA could be reduced by at least another order of magnitude. If the large background arises from Rayleigh scattering, a double monochromator with better stray light rejection will provide a solution. The incorporation of better detectors such as charge coupled devices (CCD) can help capture the elusive signals. Thus with few modifications in the optics and detection system and the endurance of ROA spectroscopists, ROA technique can emerge into one of real conformational value.

BIBLIOGRAPHY

1. S.F.Mason in "Topics in Stereochemistry", N.A.Allinger and E.L.Eliel, Eds., Wiley Intersience, New York, vol.9, pp 1-29, (1976).

2. J.Applequist, Amer.Sci., 75, 58,(1987).

3. F.A.Jenkins and H.E.White, "Fundamentals of Optics", Mcgraw Hill, New York, chapter 24, (1976).

4. B.Testa in "Studies in Organic Chemistry", P.G.Gassman, Ed, Marcel Dekker, Inc., New York, vol.6, p 5-6,69, (1979).

5. H.H.Willard, L.L.Merritt, J.A.Dean and F.A.Settle, "Instrumental Methods of Analysis", Wadsworth publishing company, CA, sixth edition, chapter 14, (1981).

6. A.Cotton, Compt.Rend., 120, 989,1044 (1895).

7. P.Crabbe and A.C.Parker in "Physical Methods of Chemistry", Part III C.- Polarimetry, A.Weissberger and B.W.Rossiter, Eds., Wiley-Interscience, vol.I,chapter3, (1971).

8. P.Crabbe in "Topics in Stereochemistry", N.L.Allinger and E.L.Eliel, Eds.,Interscience Publication, New York, Vol.1, p 93, (1967).

9. Hsu,E.C. and Holzworth,G., J. Chem.Phys. 59, 4678, (1973).

10. Holzworth.G., Hsu.E.C., Mossher.H.S., Faulkner.T.R., and Moscowitz.A., J.Am.Chem.Soc., 96, 251, (1974).

11. L.A.Nafie and T.A.Freedman in "Topics in Stereochemistry", E.L.Eliel and S.H.Wilen, Eds., Interscience Publication, New York, vol.17, p 113, (1987) and references therein.

12. J.S.Cheng, L.A.Nafie, S.D.Allen and A.I.Braunstein., Appl.Opt, 15, 8, (1976).

13. M.Diem, G.M.Roberts, O.Lee and A.Barlow, Appl.Spectrosc.,42, 20, (1988) and references therein.

14. P.J.Stephens, J.Phys.Chem.89, 748,(1985).

15. G.W.Chantry in "The Raman effect", A.Anderson, Ed., Marcel Decker Inc., New York, Vol.1, p 49-50, (1971).

16. P.W.Atkins and L.D.Barron., Mol.Phys., 16, 453, (1969).

17. L.D.Barron and Buckingham., Mol.Phys., 20,1111, (1971).

18. L.D.Barron, M.P.Boggard and A.D.Buckingham., J.Am. Chem.Soc.,95, 603, (1973).

19. W.Hug.,Appl.Spectrosc., 35,115, (1981).

20. L.D.Barron and Vrbancich., J.Raman.Spectrosc, 15, 47, (1984).

21. Reza Oboodi, M.A.Davies, U.Gunnia, M.B.Blackburn and M.Diem.,J.Raman.Spectrosc.,16, 366, (1985).

22. L.D.Barron., Nature, 257, 372, (1975).

23. T.R.Devine and T.A.Keiderling., J.Phys.Chem.,88,390, (1984).

24. W.Kauzmann, "Quantum Chemistry", Academic Press, New York, p 548-549, (1957).

25. A.Moscowitz in "Advances in chemical physics", I.Prigogine, Ed., Interscience Publication, New York, vol.IV, p 67-80, (1961).

26. M.Diem, Ph.D. Dissertation, University of Toledo, (1976).

27. L.D.Barron and Buckingham - Annu.Rev.Phy.Chem.,26, 381, (1975).

28. L.D.Barron - Adv.Inf.Red.Raman Spectrosc.,4, 271, (1978).

29. L.D.Barron in "Molecular Spectroscopy", vol 4 - R.F.Burrow, A.D.Long, and D.J.Miller, Ed., The Chemical Society, London, p 96, (1976).

30. L.D.Barron, "Molecular Light Scattering and Optical Activity", Cambridge University Press,Cambridge,(1982).

31. A.D.Buckingham and R.E.Raab, Proc.Roy.Soc., A 345, 365, (1975).

32. L.D.Barron and J.R.Esribano, Chem.Phys.,98, 437, (1985).

33. J.A.Schellman, J.Chem.Phys.,44, 1, (1966).

34. L.D.Barron, J.Chem.Soc.,(A) 18, 2899, (1971).

35. L.D.Barron, Nature 238, 5358, (1972).

36. L.D.Barron and A.D.Buckingham - Ann.Rev.Phys.Chem., 26, 381, (1975).

37. G.Holzworth and I.Chabay., J.Chem.Phys. 57, 1632, (1972).

38. J.A.Schellman, J.Chem.Phy., 58, 2882, (1973).

39. T.B.Freedman and L.A.Nafie, J.Chem.Phy., 78, 27, (1983).

40. L.D.Barron and A.D.Buckingham., J.Am.Chem.Soc., 96, 4769, (1974).

41. L.D.Barron and A.D.Buckingham., J.Am.Chem.Soc., 101, 1979, (1979).

42. L.D.Barron and B.P.Clark., Mol.Phys., 46, 839, (1982).

43. L.D.Barron, J.R.Escribano and J.F.Torrance., Mol.Phys., 57, 653, (1986).

44. H.Boucher, T.R.Brocki, M.Moskovitz and B.Bosnich., J.Am.Chem.Soc., 99, 6870, (1977).

45. W.Hug and H.Surbeck., Chem.Phys.Lett., 60, 180, (1979).

46. U.Gunnia, M.Davies and M.Diem, J.Raman Spectrosc., 18, 399, (1987).

47. M.Diem, F.Adar and R.Grayzel., Computer Enhanced Spectrosc., 3, 29, (1986).

48. M.Born and E.Wolf, "Principles of Optics", Pergamon Press, New York, p 28, (1970).

49. T.B.Freedman, J.Kallmerten, C.G.Zimba, W.M.Zuk, and L.A.Nafie, J.Am.Chem.Soc., 106, p 1244, (1984).

50. J.Calienni, M.Davies, U.Gunnia and M.Diem, J.Phys. Chem., submitted for publication, (1988).

51. G.Forrest and R.C.Lord, J.Raman Spectrosc., 6, 32, (1977).